Investigation and comparison of the energy storage performance of MXenes in dilute aqueous electrolytes and highly concentrated water-in-salt electrolytes

A Thesis

submitted in partial fulfillment of the requirements of the

BS-MS Degree (2017-2022)

At the

Indian Institute of Science Education and Research Pune
India – 411008

By

Atharva Harshawardhan Ladole

BS-MS 5th Year
Registration # 20171208

Supervisor: Dr. Beatriz Mendoza Sánchez
Institute for Applied Materials – Energy Storage Systems (IAM-ESS),
Karlsruhe Institute of Technology, Germany

Expert: Dr. Muhammed Musthafa
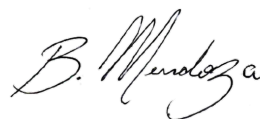Indian Institute of Science Education and Research Pune, India

Certificate

This is to certify that this dissertation entitled **"Investigation and comparison of the energy storage performance of MXenes in dilute aqueous electrolytes and highly concentrated water-in-salt electrolytes"** towards the partial fulfilment of the BS-MS dual degree programme at the Indian Institute of Science Education and Research, Pune represents study/work carried out by **Atharva Harshawardhan Ladole** at Institute of Applied Materials - Energy Storage Systems, Karlsruhe Institute of Technology, Germany under the supervision of **Dr. Beatriz Mendoza Sánchez, IAM-ESS Karlsruhe Institute of Technology, Germany** during the academic year 2021-2022.
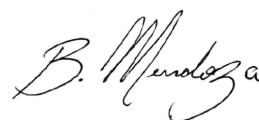
Atharva Harshawardhan Ladole   Dr. Beatriz Mendoza Sánchez

Declaration

I hereby declare that the matter embodied in the report entitled **"Investigation and comparison of the energy storage performance of MXenes in dilute aqueous electrolytes and highly concentrated water-in-salt electrolytes"** are the results of the work carried out by me at the Institute of Applied Materials – Energy Storage Systems, Karlsruhe Institute of Technology, under the supervision of **Dr. Beatriz Mendoza Sánchez** and the same has not been submitted elsewhere for any other degree.

Atharva Harshawardhan Ladole   Dr. Beatriz Mendoza Sánchez

Acknowledgement

I place on record my sincere thanks to Dr. Beatriz Mendoza Sánchez for this opportunity to work at Karlsruher Institut für Technologie, Germany, on my master's thesis, and her constant encouragement and support, which helped me to carry out my project with utmost success.

I am thankful for the stimulating and insightful lunchtime discussions with my labmates Enrique Samperio Niembro and Tianzhu Liu, on a vast range of topics including but not limited to academia, and for having me in their care.

I will be forever grateful to my roommates at O3-HaDiKo, without whom I wouldn't at all have a life outside of my lab, and for the chance to experience a "college life" in the beautiful city of Karlsruhe, which I missed out on in while studying in India.

I owe it to IISER faculty and the courses offered by them, and my past projects at NCL, IISc, and IISER which made me capable to understand advanced concepts, tackle research problems with clear fundamental knowledge, and provided me a thorough laboratory experience with different instruments and techniques allowing me to come up with ingenious solutions to problems faced in experiments.

Lastly, I want to thank my family and friends for their constant support and motivation, my parents Dr. Smita Ladole and Harshawardhan Ladole, and my dear sister Sailee Ladole for believing in me and my dreams, keeping my morale high in stressful times, and enabling me to hustle with hard work to make them, and myself, proud of me. Without them, I couldn't possibly have accomplished this project, thus, I dedicate my thesis to them:)

Contents

Abbreviations

LiTFSI	Lithium bis(trifluoromethanesulfonyl)imide
LiBETI	Lithium bis(pentafluoroethanesulfonyl)imide
LiSFSI	Lithium sulfonylbis(fluorosulfonyl)imide
Mg(TFSI)$_2$	Magnesium bis(trifluoromethane sulfonyl)imide
KAc	Potassium acetate
LiAc	Lithium acetate
PTFE	Polytetrafluoroethylene
rpm	Rotations per minute
N$_2$	Nitrogen gas
DI	De-ionized water
TMAOH	Tetramethylammonium hydroxide

List of Figures

List of Tables

Abstract

In this thesis, the pseudocapacitive performance of V_2C MXene in different aqueous and acidic electrolytes was investigated. V_2C was found to have the highest capacitance, even greater than $500\,F/g$, with $3\,M$ and $1\,M$ H_2SO_4. The two pairs of pseudocapacitive peaks of V_2C observed in windows A (from $-0.65\,V$ to $-0.27\,V$ vs Ag/AgCl) and B (from $-0.27\,V$ to $0.26\,V$ vs Ag/AgCl) were studied, and conclusions were made about the stability of these two electrochemical processes. Dilute aqueous electrolytes based on nitrate, chloride, sulphate anion salts were studied, and among these, V_2C was found to perform the best in the lithium and potassium ion salts at higher scan-rates. At very low scan rates we examined a peculiar pseudocapacitive storage from some magnesium ion salts. Further, suitable Li^+ and K^+ salts are chosen with high enough solubility, to prepare cheap, non-toxic water in salt electrolytes (WiSE). A remarkable cyclic stability of V_2C is observed in some WiSE, particularly the lithium ion based WiSE display an electrochemical stability window (ESW) larger than $1.23\,V$. Enhancing ESW along with good capacity allowed to improve energy density of V_2C MXene.

1. Introduction

The inevitable technological advancement has allowed technology to penetrate each and every aspect of our daily lives regardless of whether we belong to a developed or developing economy. Consequently, to keep up with the surging energy consumption worldwide, economies are investing in renewable energy sources, to sustain the energy demands in the long term. However, most renewable energies like solar, wind, tidal, geothermal and hydro powered are intermittent by nature, which creates a need to store these energies [1]. Apart from this, with more and more technologies becoming portable, energy storage devices are the simplest way to power them.

We realize the crucial role energy storage devices play in this high-tech world, thus fostering a widespread research interest in their development. Depending on their application, some energy storage devices are better suited than others. Supercapacitors are a class of electrochemical energy storage devices known for their high power density, good cycling stability (*Figure 1*). These properties make them suitable not only for delivering bursts of power for example to accelerate a motor, but also to charge with these spasmodic potentials in regenerative braking, electrical grids, triboelectric generators, wind turbines, and other intermittent energy sources where large influxes of energy needs to be handled rapidly.
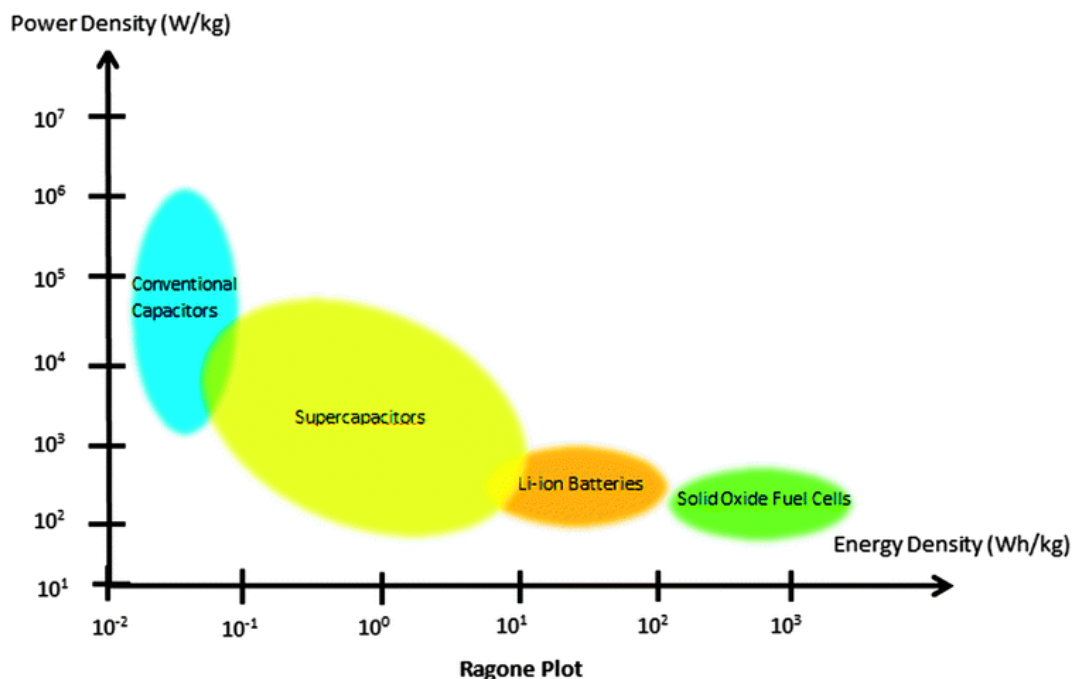
Figure 1: Comparison of different energy storage devices on a Ragone plot. [2]

1.1 Comparison of electrostatic with supercapacitive energy storage

An electrostatic capacitor stores charge Q on two parallel plates separated by a dielectric, which increases linearly with a constant slope in proportion to the potential difference between the plates ΔV, limited only by the breakdown voltage of the dielectric.

$$Q = C\Delta V$$

<div align="right">Equation 1</div>

where the slope is the capacitance C, which can be quantified from the relation,

$$C = \varepsilon_r \varepsilon_0 \frac{A}{d}$$

<div align="right">Equation 2</div>

Where ε_r is the relative permittivity of the dielectric, ε_0 is the permittivity of vacuum, A is the area of each of the parallel plates separated by distance d. The energy (E) in this case is stored in the form of an electric field and is given by the relation,

$$E = \frac{1}{2}C\Delta V^2$$

<div align="right">Equation 3</div>

Electrochemical capacitors (ECs), also known as supercapacitors, can be broadly classified into two categories based on the charge storage mechanism.

The electrochemical double layer capacitors (EDLCs) where energy is stored at the interface of the electrode in contact with the electrolyte through reversible ion adsorption charging the "double layer capacitance". This double layer consists of, an electron rich or deficient layer within the surface of the solid electrode exposed to the electrolyte, and a layer of opposite polarity forming from dissolved ions in a solvated state in the electrolyte. These two oppositely charged layers are separated by a single layer of solvent molecules physically adsorbed on the electrode surface acting like a "molecular dielectric". The charge density across this double layer can be explained by different models like the Helmholtz-Perrin model, Gouy-Chapman model, Stern Model, Grahame model, etc., each model having their own merits. These EDLCs represent over 80% of the commercially manufactured electrochemical capacitors (ECs) today [3].

Another important category of ECs known as pseudocapacitors undergo 2D faradaic charge transfer processes involving monolayer or quasi-monolayer of electrochemically reactive species formed on the electrode electrolyte interface. The charge transfer processes occur at active sites which are very close to the electrode surface and thus, these processes are not limited by diffusion of electrolyte ions into the bulk of the electrode, allowing for fast charge and discharge. This intermediate process is fundamentally different than those in battery materials in terms of the linear response of voltage to the change in charge and conversely when subjected to linearly changing potential, a nearly constant capacitive charging/discharging current (i) arises, resembling an electrostatic capacitor [4,5] (*Figure 2*). This $i - V$ response at different potential sweep-rates (v) can be visualized from the relation [6,7]

Figure 2: Typical i-V plots of a capacitor and a battery [5].

$$i = av^b$$

Where i (mA) is the current observed at scan rate v (mVs^{-1}), with parameters a and b. For capacitive process, as discussed earlier, $i \propto v$, giving the value of b to be $1^{[5]}$. The high degree of kinetic reversibility of supercapacitor processes resembles electrostatic capacitors.

1.2 Challenges

Material irreversibility and kinetic irreversibility is commonly seen in battery materials, with the irreversibility between anodic and cathodic sweeps increasing with the sweep-rate [4], shortening their cycle life and making them unsuitable for high power applications. Pseudocapacitive materials hold the potential to achieve high energy densities while maintaining the EDLC like cycle life and power density. Their performance and feasibility are highly dependent on the electrode material, electrolyte, fabrication technique and scalability of the process. Popular pseudocapacitive materials like transition metal oxides, transition metal sulphides, transition metal nitrides, and conducting (conjugated) polymers, possess high theoretical capacitance but often suffer from degradation due to loss in conductivity,

reversibility, rate capability etc. The use of binders to fabricate composite electrodes, macro scale electrodes, or to bind the active material to the current collector also limits the conductivity of the material [8]. Gas evolution from exceeding the stable potentials of the electrolyte can be detrimental to not just the material by delamination and pinholes increasing the resistance, but also to the device cell, with the gas under pressure in the encapsulation, waiting to explode [9]. Considering this, aqueous electrolytes, due to the narrow electrochemical stability window of $1.23V$ imposed by electrolysis of water, limit the energy density of the device. Thereby, organic electrolytes, due to their ability to endure high voltages, are a common choice to extract high energy density from an electrode material. Although, there are concerns of cost, safety and toxicity associated with these electrolytes with them being an environment hazard, inflammable, and requiring special dry environment manufacturing processes [10,11].

1.3 Planned approach

Addressing the aforementioned challenges, in this thesis I approach these problems in two ways.

1.3.1 Using two dimensional MXene as an electrode material

Two-dimensional (2D) materials like graphene, phosphorene, hexagonal boron nitrides, metal oxides and hydroxides, and transition metal dichalcogenides are solids possessing few atomic layer thicknesses and gained tremendous interest due to their unique and exceptional mechanical, optoelectronic, and catalytic properties, and large surface area as compared to their bulk parent material.

Discovered in 2011, a large group of early transition metal carbides, nitrides and carbonitrides, referred to as MXenes [12], have been identified as a new class of 2D materials and have opened up new perspectives in advanced flexible, miniaturized and ultrathin energy storage devices with high energy and power densities [13-15]. MXenes are produced by selectively etching out "A" layers from the "MAX" phase. The name "MAX" is derived from its composition, namely, $M_{n+1}AX_n$, where M is an early transition metal, A is mainly a group 13 or 14 element, X is C (carbon) and/or N (nitrogen), and n = 1, 2, or 3. The resultant MXene which can be represented as $M_{n+1}X_nT_x$, where T stands for the various possible surface-terminating functional groups (OH, F, O, H, etc.).

These functional groups allow the surface of the 2D material to have a variety of chemistries which can be selected and modified to a great extent, which in addition to its exceptional properties like intrinsic high surface area and metallic conductivity, makes it an attractive material for applications involving ion intercalation and pseudo capacitance. The intrinsic high mechanical strength and packing densities of 2D materials with the ease of solution processing of MXenes makes them an ideal candidate for miniaturized, flexible and ultrathin energy storage devices.

Previous reports describe the favorable properties of few MXenes for energy storage applications [13,16], displaying high-rate pseudocapacitive energy storage [17]. However, most of these reports are focused on Ti_3C_2, while more than 20 other MXenes have not yet been investigated in the context of energy storage. Among these, M$_2$X type MXenes with low formula weights, are theoretically predicted to have better gravimetric performance [16,18-19].

In this thesis, I investigate V_2C MXene as an electrode material, studies on which are scarce due to its challenging synthesis, but has been reported to display excellent gravimetric performance as a supercapacitor electrode with aqueous electrolytes [20-24].

1.3.2 Using highly concentrated water-in-salt electrolytes (WiSE)

Recently proposed highly concentrated "water-in-salt" electrolytes (WiSE) [25] display stability even in high voltages as compared to conventional aqueous electrolytes by kinetic suppression of hydrogen evolution reaction (HER) and oxygen evolution reaction (OER). These highly concentrated aqueous solutions, where the salt comprises the majority of the mass and volume of the solution system, decrease the activity of water molecules since all water molecules are a part of ion solvation shells leaving no "free" water, which is responsible for the extension of their electrochemically stable potential windows. These high voltage electrolytes are attractive substitutes for the hazardous organic electrolytes and have already shown excellent results with aqueous batteries [26] and supercapacitors [27]. These demonstrations have been done commonly using fluorinated imide-based electrolytes like $LiTFSI$, $LiBETI$, $LiSFSI$, $Mg(TFSI)_2$, which are expensive to produce and potentially toxic.

In this thesis, I explore WiSE based on safe, low-cost and highly soluble KAc [28,29], $LiAc$ [29], $LiCl$ [30,31] and $LiBr$ [30] salts which have very few reports of being used with

pseudocapacitive electrodes and have not been reported at all with V_2C MXene. These electrolytes with a larger stability window will significantly improve the energy density of the material as a result of the quadratic relationship between energy density and potential (*Equation 3*).

There have been few studies about the pseudocapacitive performance of MXenes in WiSE, even so, mostly on titanium carbide MXene and $LiTFSI$ WiSE [14, 32-38].

1.4 General objective

To investigate the energy storage properties of V_2C in aqueous electrolytes and WiSE.

1.5 Objectives

i. To investigate the energy storage properties of V_2C in low concentration aqueous electrolytes. The study of electrolytes considers classification according to the anion (*Table 1*).

ii. To investigate in-depth the energy storage properties of V_2C in sulfuric acid. Different electrolyte concentrations are considered.

iii. To investigate the energy storage properties of V_2C, in a range of selected WiSE electrolytes (*Table 1*).

Energy storage properties are investigated using cyclic voltammetry in three-electrode cells. Focus is kept on studying overall storage performance as a function of scan rate. Special attention is kept on investigation of energy storage process in place (EDLC or pseduocapacitance). Electrolyte properties such as concentration, pH and conductivity are correlated with energy storage properties.

2. Characterization techniques

Given in this section is a general understanding of the equipment and characterization techniques used in this thesis.

2.1 X-Ray Diffraction

X-Ray radiation has wavelength (λ) of an order of magnitude similar to the interatomic distances in a crystalline material. Thus, a crystal can in principle behave as a 3D diffraction grating to the X-Rays, which can undergo constructive and destructive interference upon scattering, forming intense peaks, depending on the angle of incidence with respect to the crystal lattice. These angles can be determined using Bragg's law, $2d_{hkl} \sin \theta = n\lambda$, where, d_{hkl} is the interplanar distance among the family planes with miller index $\{h\,k\,l\}$, n is the diffraction order, θ is $\pi/2$ minus the angle between incident X-Ray and $< h\,k\,l >$ family of directions, λ is the wavelength of the incident X-Rays. From the θ corresponding to intense scattering (constructive interference), we get information about the possible miller planes, and consequently, the compositional and crystallographic phase of a crystalline material.

2.2 Scanning electron microscopy

The surface morphology of a material can be studied using a scanning electron microscope (SEM) which constructs images from the secondary electrons emitted from the top few nanometers of the surface when subjected to a very narrow electron beam. These SEM micrographs have a large depth of field giving us sharp images giving us a 3D understanding of the material surface. The samples should be electrically grounded and the surface should be/made conductive to prevent charge accumulation.

Figure 3: A scanning electron microscope.

2.3 Cyclic voltammetry

A cyclic voltammogram (CV) is in principle a $i-V$ plot where the current (i) response of a working electrode material is measured against an applied potential (V) changing at a constant set scan/sweep rate (v) between the stable minimum and maximum potential limits ($V_1\ and\ V_2$ respectively), keeping the electrode setup still and electrolyte unstirred so that diffusion controlled redox activity could be studied.

In the context of capacitors, their capacitance (C) can be determined from this measurement using the relations,

$$C = \frac{\Delta Q}{\Delta V} \Rightarrow C = \frac{\int_{V_1}^{V_2} i(V) dt}{V_2 - V_1} \Rightarrow C = \frac{v \times \int_{V_1}^{V_2} i(V) dt}{v \times (V_2 - V_1)}$$

$$\Rightarrow C = \frac{\int_{V_1}^{V_2} i(V) dV}{v(V_2 - V_1)} \left(\because v = \frac{dV}{dt} is\ a\ constant, vdt = dV\right)$$

$$\Rightarrow C = \frac{absolute\ area\ under\ the\ i-V\ plot}{scanrate \times (potential\ window)}$$

A *BioLogic VMP300* potentiostat is used for the electrochemical characterization in three-electrode configuration, where the current flow is between the working-electrode (WE) and counter-electrode (CE), and the potential is applied and measured between the WE and the reference-electrode (RE). The RE, as its name suggests, has a known electrochemical redox potential, and this stable reaction serves as a reference to modify or measure the potential of the WE against.

3. Experimental

3.1 Synthesis of multilayered MXene

The MAX phase used in this thesis is V_2AlC which was synthesized by our collaborators at *Drexel University* in a solid-state reaction. We use this MAX phase as obtained in a powder form to synthesize two-dimensional V_2C (vanadium carbide) MXene. To ensure that there are no clumps in the MAX powder, it is sieved through a $36\,\mu m$ stainless steel mesh, homogenizing the powder by particle size.

3.1.1 Etching of MAX phase

As a first step, we need to etch out the A layers, which in this case is aluminium, from the V_2AlC powder using an etchant. We add $1\,g$ of V_2AlC in an etchant mixture of $12\,mL$ of 48% HF (w/w) and $8mL$ of 37% (w/w) HCl stirring at $350\,rpm$ in a PTFE reaction vessel, on a hotplate set at $35\,°C$. The reaction of MAX with the etchant is highly exothermic. Due to this reason, it is essential that the MAX powder be added slowly in small amounts over a period of 10 minutes. We leave this reaction mixture stirring in an oil bath for 4 days to allow enough time for the etchant to react deeply with the bulk of the MAX particles.
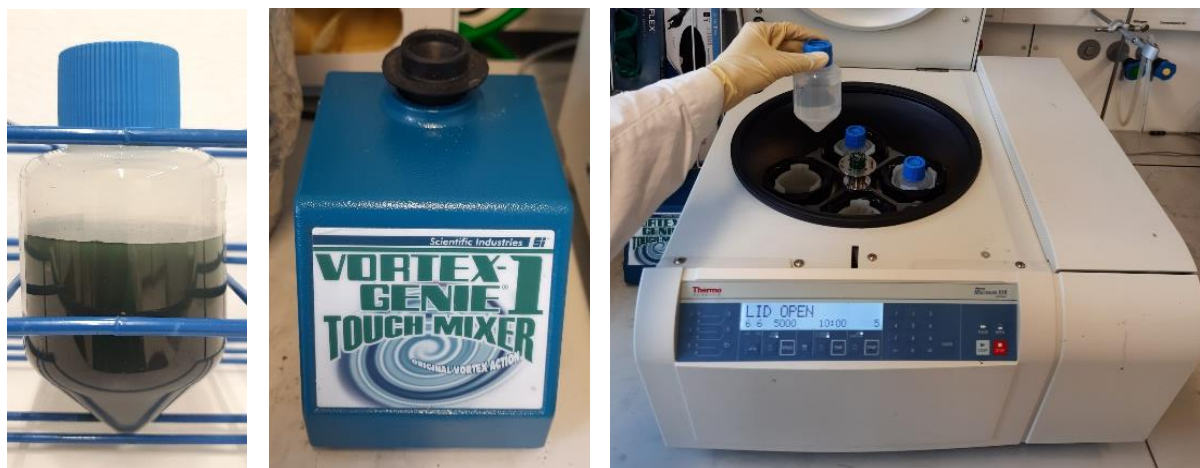
Figure 4:(a) The reaction mixture in the centrifuge tube, (b)Vortex mixer, (c)Centrifuge

3.1.2 Washing off the etchant

After 4 days of stirring, the reaction mixture ($\sim 20mL$) is carefully transferred to a $150\,mL$ centrifuge tube filled with $120\,mL$ DI water bubbled with N_2. The DI water is bubbled with N_2 to reduce the possibility of oxidation of the sensitive MXene by displacing the dissolved oxygen in water. The volume of the diluted mixture is made $150\,mL$ by adding more water and the mixture is mixed thoroughly by manually

shaking it vigorously and with the assistance of a vortex mixer. This tube is centrifuged in a *Thermo Scientific™ Multifuge X1R* refrigerated centrifuge for 10 minutes at $5000\ rpm$ maintained at a low temperature of $5\ ℃$ (*Figure 4*). After completion of centrifugation, a few drops of the supernatant are pipetted out to measure its pH using a pH-paper, and the rest of the supernatant is carefully discarded in HF waste using a pipette. The etched MAX phase precipitate is composed of loosely packed, stacked particles with an accordion-like structure called multilayered, or ML-MXene which can be represented as $M_{n+1}X_nT_x$, where T stands for the various possible surface-terminating functional groups (OH, F, O, H, Cl etc.). The centrifuge tube with the precipitate in it is again filled with DI water and the precipitate suspended again by shaking to wash away more and more acid from the bulk of the ML-MXene. This mixture is centrifuged again at the same parameters and the pH of the supernatant is measured again. This washing process is repeated (*Figure 5*) until the pH of the supernatant obtained is at a nearly neutral level (*pH between 6 and 7*).
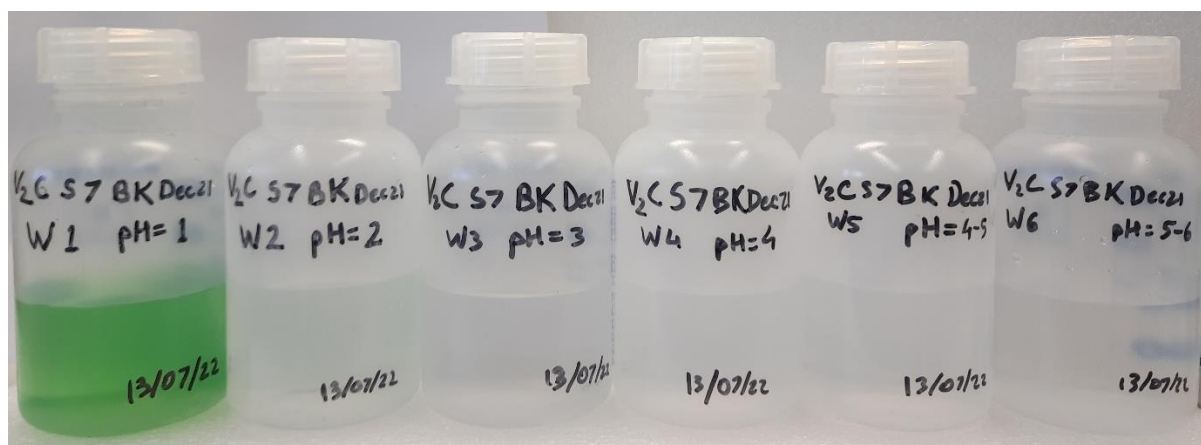
Figure 5:The supernatants from all the washes with increasing pH

3.1.3   Obtaining the ML-MXene

After we get a near neutral pH value from the supernatant, we suspend this precipitate in DI water for one last time before we finally filter this suspension through a vacuum filtration setup using a $0.45\ \mu m$ pore sized PTFE membrane filter. The obtained residue is a wet ML-MXene powder which is weighed and a calculated fraction of which is dried in vacuum at room temperature for characterization, and the rest of the wet ML-MXene powder used in the next step.

If 1 g of V_2AlC is etched with 100% efficiency with the reaction,

$$2\,V_2AlC + 6HF \rightarrow 2V_2C + 2AlF_3 + 3H_2 \uparrow$$
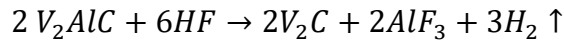
we should theoretically get 0.81 g of V_2C. However, the actual product is V_2CT_x and we do not have the information about which surface terminations are present and in what ratios. There is also some unetched MAX phase present in the product making it very difficult to determine a yield at this stage of synthesis.

3.1.4 Delamination of ML-MXene

The replacement of the strong $Al-M$ bonds of the MAX phase by weaker hydrogen or van der Waals bonds allows for the facile delamination of MXene.

3.1.5 Intercalation of organic molecule

The obtained wet ML-MXene powder is added to a mixture of $3.88\,mL$ of 25% (w/w) TMAOH and $15.52\,mL$ of N_2-bubbled DI water, and left to stir at $350\,rpm$ in an oil bath of $35\,°C$, for a duration of one day. In this step, the basic organic solvent TMAOH participates in an ion exchange reaction with the intercalated proton/hydronium ion in the wet multilayered MXene causing the layers to swell up with the intercalation of large TMA+ ion assisting in delamination of the multilayered MXene to individual MXene flakes [20].

3.1.6 Washing away the excess organic solvent

Removing the reaction vessel from the bath, we carefully transfer this reaction mixture to a $150\,mL$ centrifuge tube filled with $120\,mL\,N_2$-bubbled DI water, after which the tube is filled to the $150\,mL$ graduation with more DI water. This mixture is then centrifuged at $5000\,rpm$ for 20 minutes to wash away the organic solvent first to get a near neutral pH from the current strong basic pH. Similar to the step 2.1.1.2, we check the pH of the supernatant using a pH paper, and discard the rest carefully in the basic waste and repeat the centrifugation process until the pH of the supernatant goes to 7.

3.1.7 Delamination and washing.

After discarding the near neutral supernatant in the previous step, we add N_2-bubbled DI water to the centrifuge tube. Shaking this product starts the exfoliation of the multilayered MXene giving us 2-D MXene flakes, which form a stable, surfactant-free colloidal solution in water as a result of the hydrophilic nature of MXenes. We separate a little volume of the supernatant for measuring concentration using UV-Vis absorbance spectroscopy.

3.2 Obtaining 2D-MXene electrodes

3.2.1 Filtration of the 2D-MXene suspension

Figure 6: (a) Vacuum filtration setup, (b) Filtered freestanding V₂C film

Some measured volume of the first purified supernatant is filtered through a $64\ nm$ pore size *Celgard 3501* membrane in a vacuum filtration setup, and the membrane is carefully lifted off, without disturbing the residue layer formed on top of it after filtration. This membrane is now dried in vacuum at room temperature, until the residue dries completely to form a flexible, freestanding 2D-MXene film with metallic luster, which peels off the Celgard membrane with the help of a spatula (*Figure 6*). After weighing this film and measuring its thickness using *Heidenhain high accuracy length gage*, we calibrate the weight/thickness against the product of volume of the suspension filtered with its concentration from UV-Vis absorbance. This calibration allows us to have control over the thickness of the next films simply from the relative concentration of the suspension (from UV-Vis absorbance) and the volume of the suspension filtered.

3.2.2 Cutting usable electrodes

The freestanding 2D-MXene films are stored in an inert atmosphere in the glovebox to prevent oxidation of the material. We cut electrodes from the big film using a circular punching tool, or a scalpel, and weigh them before assembling the cell.

3.3 Electrolyte preparation

The following electrolyte solutions were prepared from their respective salts and solutions. The measured conductivity and pH values are indicated against the respective electrolyte.

Table 1: Electrolytes prepared with their measured conductivity and pH values.

| Group	Electrolyte	Concentration	Conductivity (mS/cm)	pH
Nitrate based aqueous electrolytes	$LiNO_3$	$5\,M$	170	8.34
	$NaNO_3$	$5\,M$	191.7	6.1
	KNO_3	$2\,M$	204.4	7.37
	$Mg(NO_3)_2$	$2\,M$	147.8	6.69
	$Al(NO_3)_3$	$1\,M$	110.6	1.64
Chloride based aqueous electrolytes	$LiCl$	$5\,M$	193	5.91
	$NaCl$	$3\,M$	182.3	7.18
	KCl	$2.5\,M$	231.7	6.52
	$MgCl_2$	$3\,M$	153	5.02
Sulphate based aqueous electrolytes	H_2SO_4	$1\,M$	329.4	0.1
	Li_2SO_4	$2\,M$	85.07	8.96
	Na_2SO_4	$1\,M$	95.66	5.47
	K_2SO_4	$0.5\,M$	83.74	8.32
	Mg_2SO_4	$2\,M$	58.08	6.26
Sulphuric acids	H_2SO_4	$3\,M$	732	-0.21
	H_2SO_4	$1\,M$	329.4	0.1
	H_2SO_4	$0.5\,M$	200.2	0.37
	H_2SO_4	$0.1\,M$	42.6	0.95
Acetate based WiSE	$LiAc$	$5\,m$		
	KAc	$15\,m$	87.09	11.08
	KAc	$21m$		
	KAc	$27.1\,m$	36.31	10.86
	$Mg(Ac)_2$	$11\,m$		
Lithium Chloride WiSE	$LiCl$	$15\,m$	101.9	4.77
	$LiCl$	$19.5\,m$	70.02	5.8
Lithium Bromide WiSE	$LiBr$	$10\,m$	186.5	7.94
	$LiBr$	$15\,m$	129.2	6.4
	$LiBr$	$19\,m$	102.8	5.47

3.4 Cell assembly
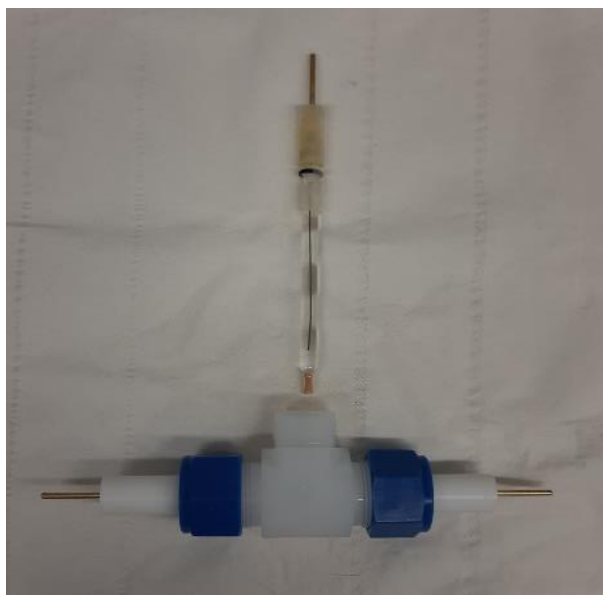
Figure 7: A three electrode swagelok cell.

The *Swagelok* cells (Figure 7) have a glassy carbon current collector surface and we cut appropriately sized electrodes from the 2D-MXene film which lie inside the glassy carbon current collector area. For the counter electrode, we use a commonly used YP-50 activated carbon, which is made to be a flat, flexible foam, from which appropriately sized activated carbon counter electrodes can be cut out for the *Swagelok* cell. *Celgard 3501* membrane has been used as the separator to isolating the two electrodes, allowing only ionic exchange.

4. Results and discussion

4.1 Synthesis

We obtain the etched ML-MXene and the free standing MXene film as products of different stages of the synthesis reaction represented in the *Figure 8*.
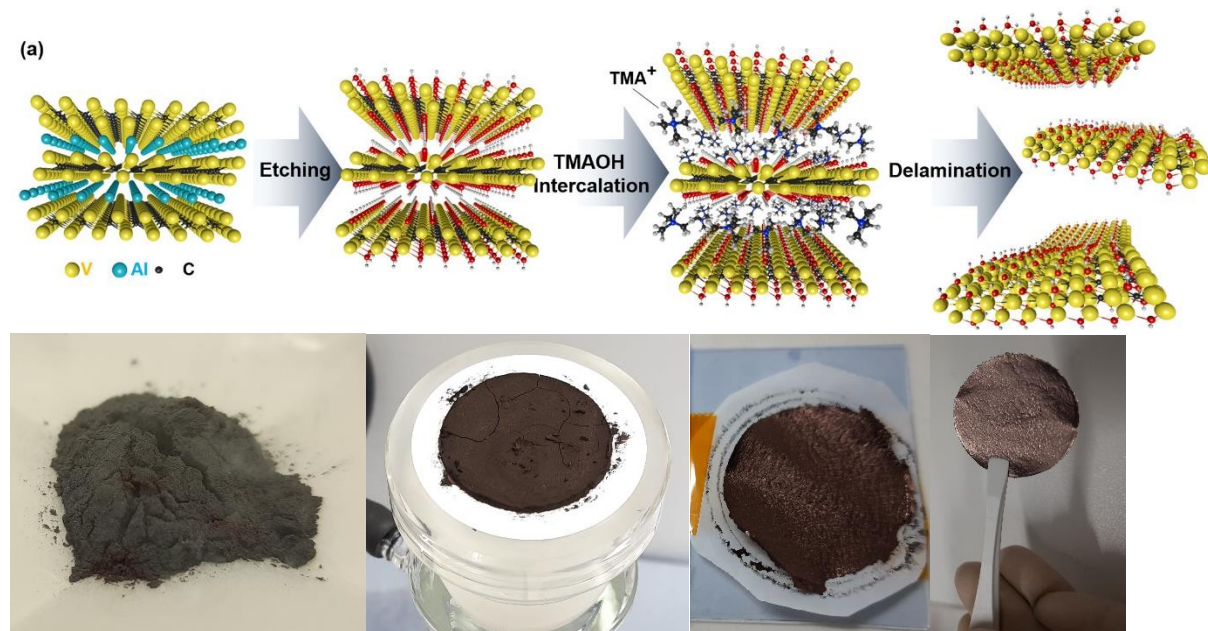

Figure 8: (a) The step-by-step synthesis process from etching of MAX phase, intercalation and delamination to obtain 2D sheets [20], (b) V₂AlC, (c) Etched V₂AlC or ML-MXene powder, (d) Filtered film from 2D nanosheets.

4.2 X-ray diffractometry

Both the filtered etched ML-MXene V_2CT_x, and the as-received starting material (MAX phase) compounds are analyzed using XRD. Comparing the XRD patterns we can see the broadening of the (002) peak after etching, due to loss in crystallinity and structural order (*Figure 9*). The *d lattice parameter* is represented by the (002), a shift in whose peak position to a lower 2θ value upon etching indicates an increase in the spacing between the hexagonal planes. This can be explained from the replacement of the strong $Al-M$ bonds of the MAX phase by weaker hydrogen or van der Waals bonds and the intercalation of water from the aqueous etchant in the layers of the 2D material.
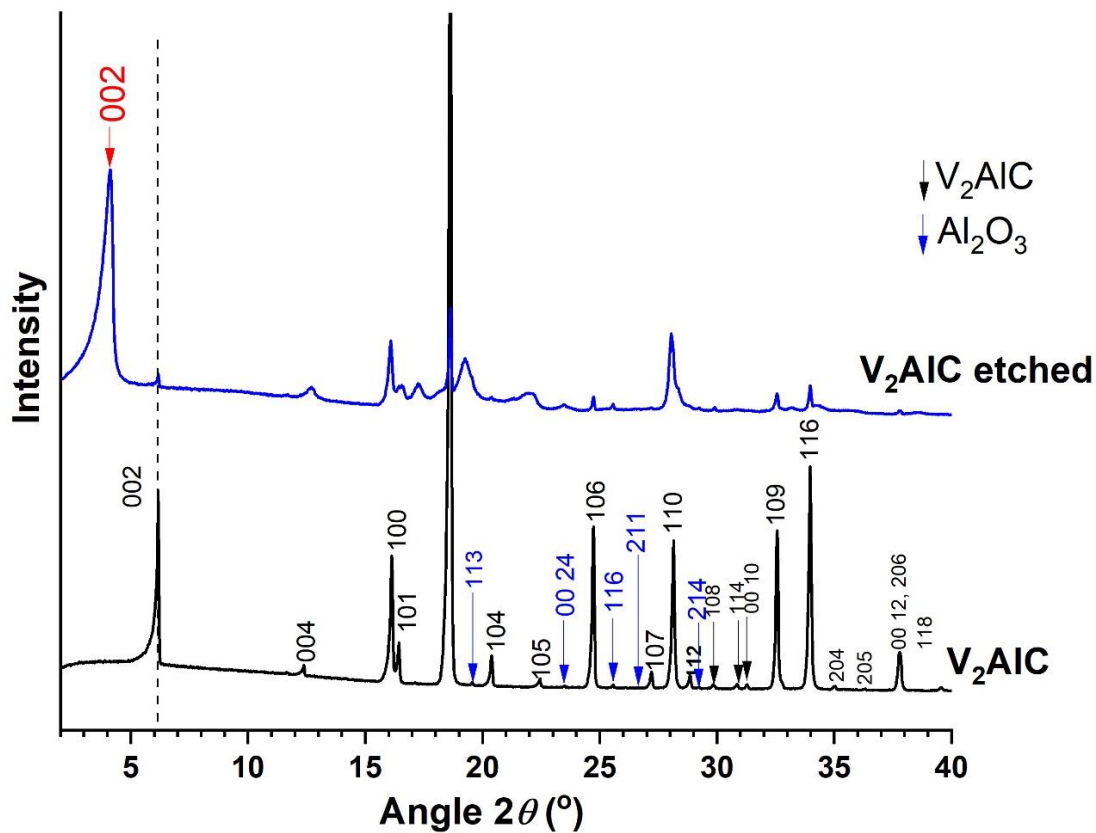
Phase	Space group	a (Å)	b (Å)	c (Å)	wt.%	R_p	R_{wp}	χ^2
V_2AlC	P 6$_3$/m m c	2.91646(2)	2.91646(2)	13.13175(3)	91.89(0.24)	3.1	4.21	3.37
V_4AlC_3	P 6$_3$/m m c	2.92697(1)	2.92697(1)	22.68779(2)	6.52(0.07)			
Al_2O_3	R -3 c	4.75482(4)	4.75482(4)	13.004(1)	1.59(0.07)			

Figure 9: XRD pattern and refinements provided by Dr. Beatriz Mendoza Sanchez

4.3 Scanning electron microscopy

The cross-sectional SEM image of the V_2C MXene film (*Figure 10*) clearly shows the nanosheets/flakes stacked in a disorderly manner as a result of vacuum filtration of the 2D MXene suspension. From the imaging software, we find that the 2D stacked layers have an interlayer spacing ranging from $155\ nm$ to $392\ nm$. This large spacing allows for some electrolyte molecules to penetrate the layers to an extent.
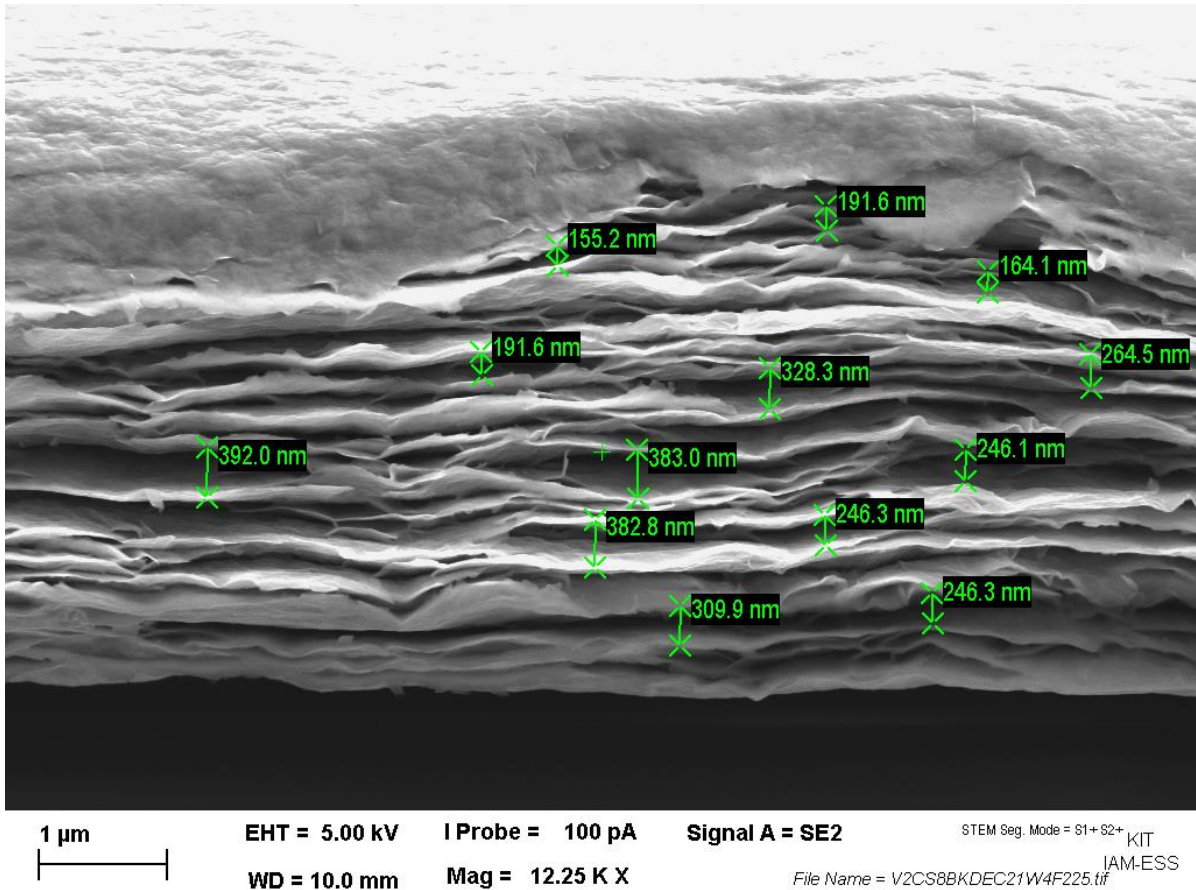
Figure 10: Cross-sectional SEM image.

4.4 Cyclic voltammetry

The stable electrochemical window selection has been done by running CVs in steps of increasing windows at very slow scan-rates, allowing enough time to reveal HER or OER taking place at any potential. These CVs and the windows selected are given as additional information in *Appendix A*.

4.4.1   Dilute aqueous electrolytes

We first investigate the electrochemical behavior of the scarcely studied V_2C MXene in common dilute aqueous electrolytes mentioned in *Table 1* to get an understanding of the pseudocapacitive response to different combinations of ions.

From the CVs in *Figure 11.* we can observe that CVs of V_2C in $5\,M\,LiNO_3$ and $5\,M\,KNO_3$ display a nearly ideal rectangular shape, characteristic of a capacitor as discussed in section 1.1. A resistive behavior is shown by the V_2C MXene in $2\,M$

$Mg(NO_3)_2$ and $1\,M\,Al(NO_3)_3$ aqueous electrolytes at a scan rate of $10\,mV/s$. Particularly in $1\,M\,Al(NO_3)_3$ we can also observe a shorter electrochemically stable window which can be explained from the measured pH of the electrolyte in *Table 1*, having an accelerated hydrogen evolution due to its acidic pH. An intermediate case between rectangular and resistive CVs is shown by V_2C in $5\,M\,NaNO_3$ at a scan rate of $10\,mV/s$.
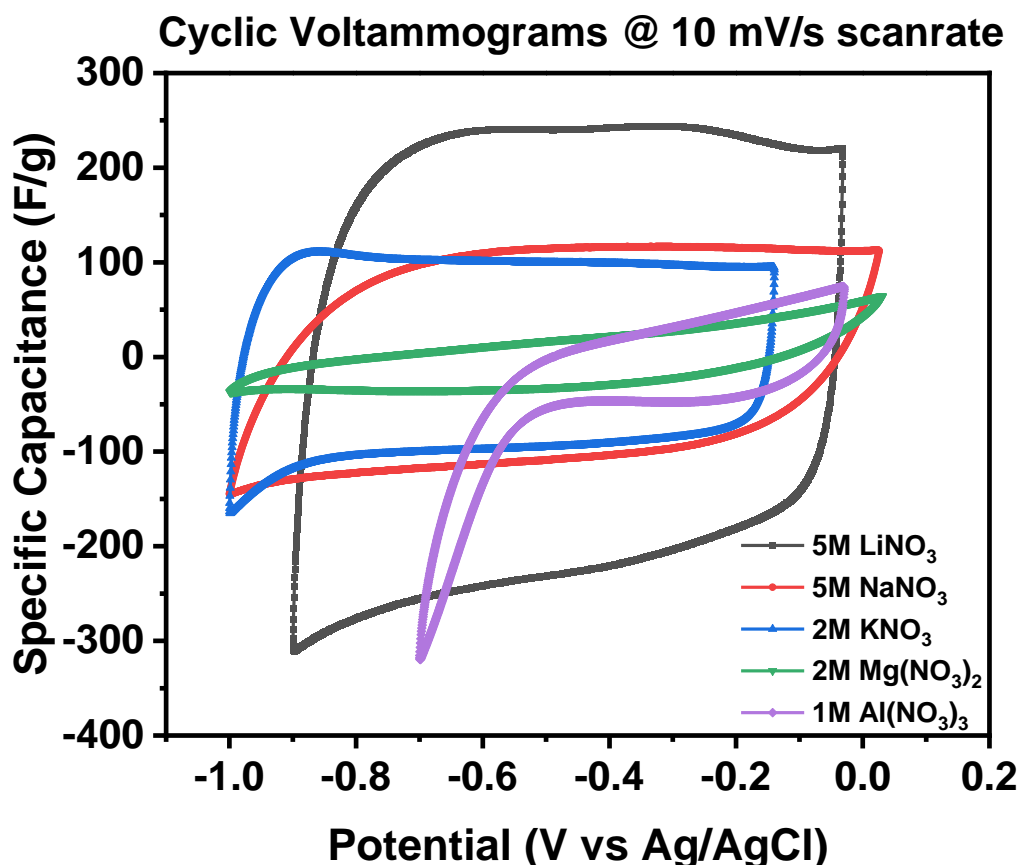

Figure 11: CVs of V₂C in nitrate based aqueous electrolytes.

Figure 12 summarizes the electrochemical performance in the form of gravimetric capacitance with respect to potential scan-rate for the nitrate anion based aqueous electrolytes. From this summary it is apparent that performance of V_2C with increasing potential scan-rate doesn't fall as sharply in $5\,M\,LiNO_3$ and $5\,M\,KNO_3$ as compared to the rapid fall in the performance in $2\,M\,Mg(NO_3)_2$ and $1\,M\,Al(NO_3)_3$ electrolytes.
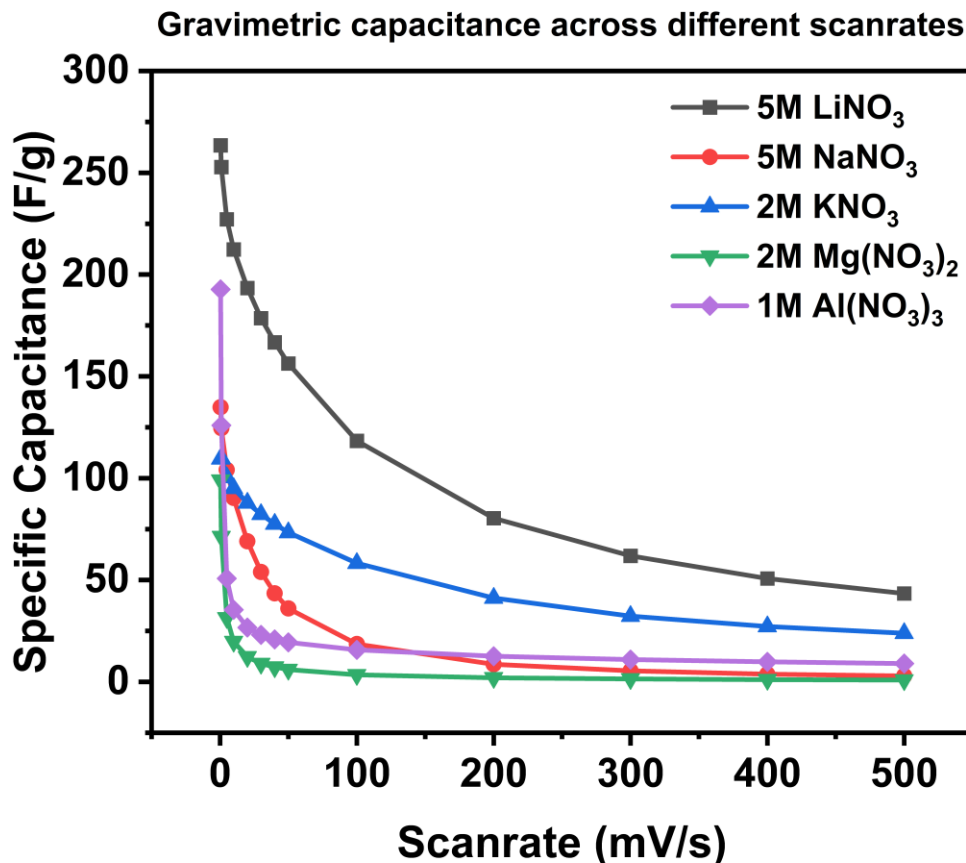
Figure 12: Capacitance vs Potential scan-rate for nitrate-based electrolytes.

This observation is supported by *Figure 11* from resistive CVs in magnesium and aluminium nitrate at moderately high scan-rate of $10\ mV/s$, implying a resistance to charge storage in these electrolytes which gets worse at higher scan-rates. The resistance to charging at faster scan is hypothesized to originate from the hinderance experienced by the bulky hydrated divalent and trivalent cations during diffusion [39], despite having a decent ionic conductivity as seen in *Table 1*.

The second group of aqueous electrolytes based on chlorides in *Figure 13* show very similar results having V_2C response in $5\ M\ LiCl$ and $2.5\ M\ KCl$ to be the closest to the ideal rectangular CV, followed by a little bit resistive $3\ M\ NaCl$ and then the much resistive $3\ M\ MgCl_2$.
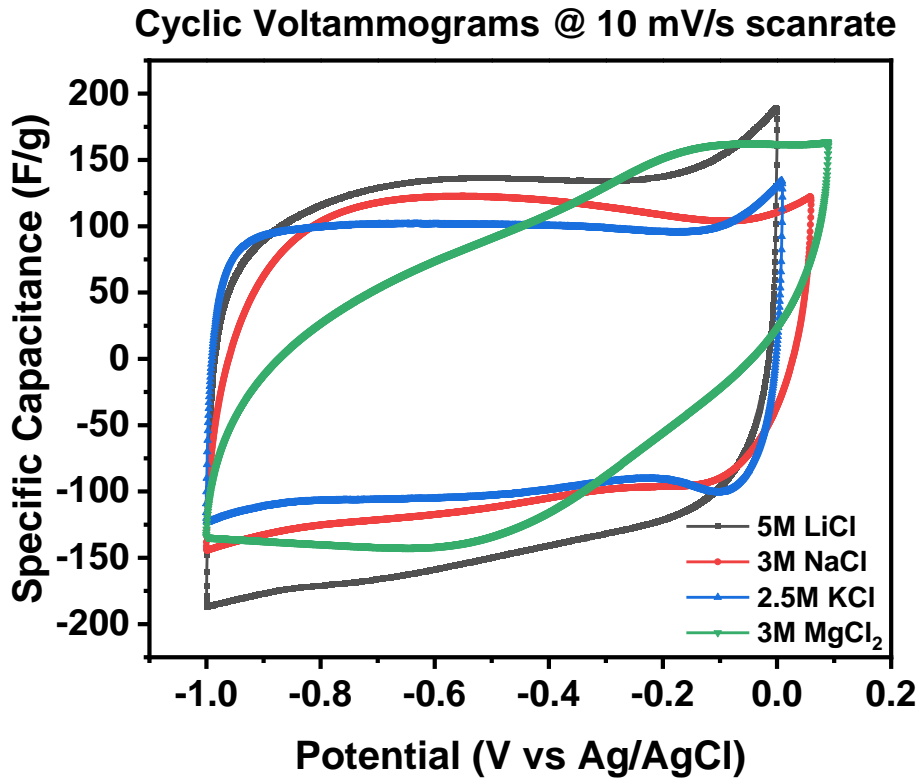
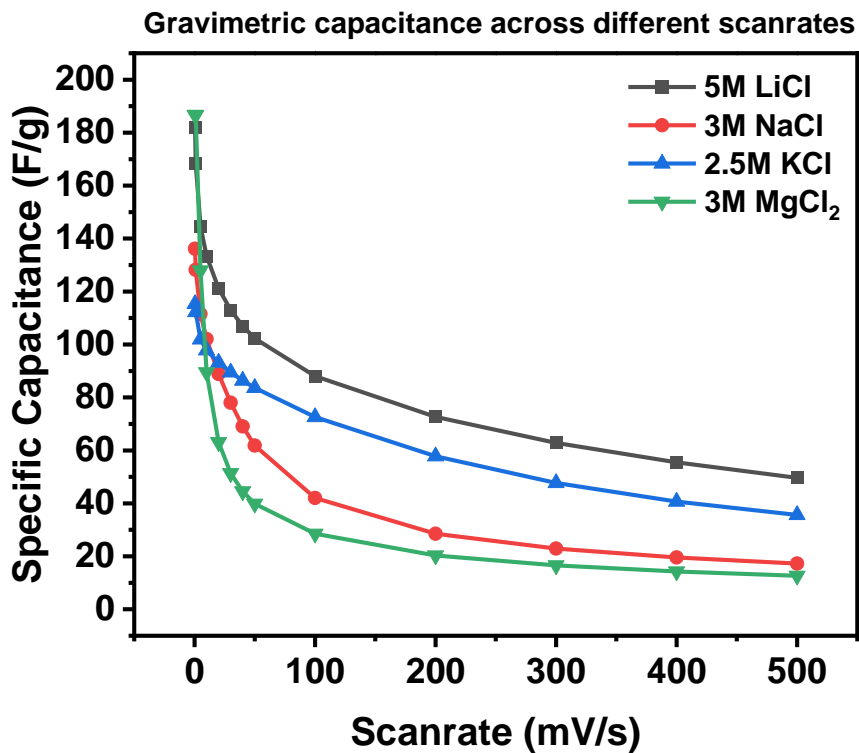*Figure 13: CVs of V₂C in chloride based aqueous electrolytes*

Figure 14: Capacitance vs Potential scan-rate for chloride based electrolytes

Again, supported by *Figure 14* V_2C in $5\ M\ LiCl$ and $2.5\ M\ KCl$ stores charge even at high potential scan-rates proving the high rate-capability of V_2C in these electrolytes. On the contrary, V_2C in $3\ M\ MgCl_2$ has the worst performance at higher scan-rates similar to what we observed previously in the case of $Mg(NO_3)_2$, with a conductivity value lowest in this electrolyte group.
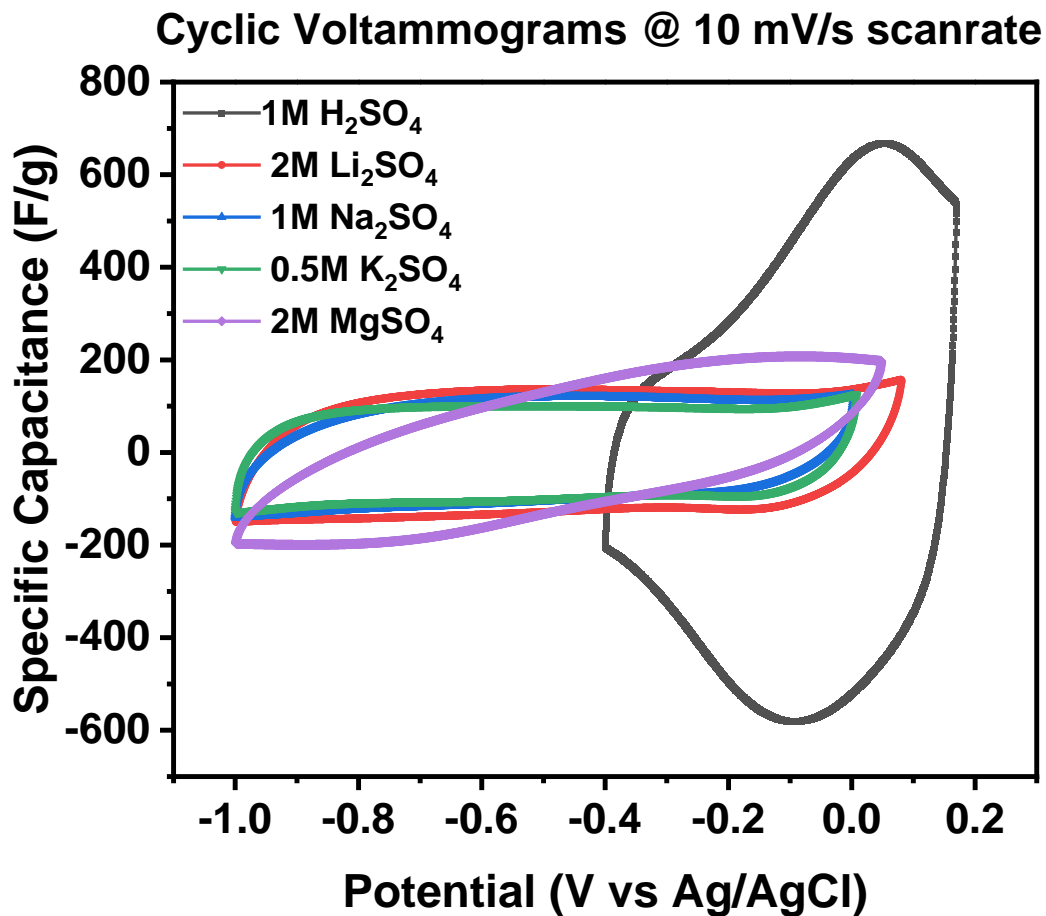
Figure 15: CVs of V₂C in sulphate based aqueous electrolytes

Aqueous sulphate based electrolytes display a similar trend in *Figure 15* For V_2C with $2\ M\ Li_2SO_4$, $1\ M Na_2SO_4$, $0.5\ M\ K_2SO_4$ having very similar rectangular CVs compared to the CV with $2\ M\ MgSO_4$ which is relatively resistive at $10\ mV/s$ scan-rate.

Figure 16 supports these observations in a similar manner showing that at high scan rates, the charge storage performance of V_2C in magnesium sulphate falls rapidly as compared to that in lithium, potassium and sodium sulphates.
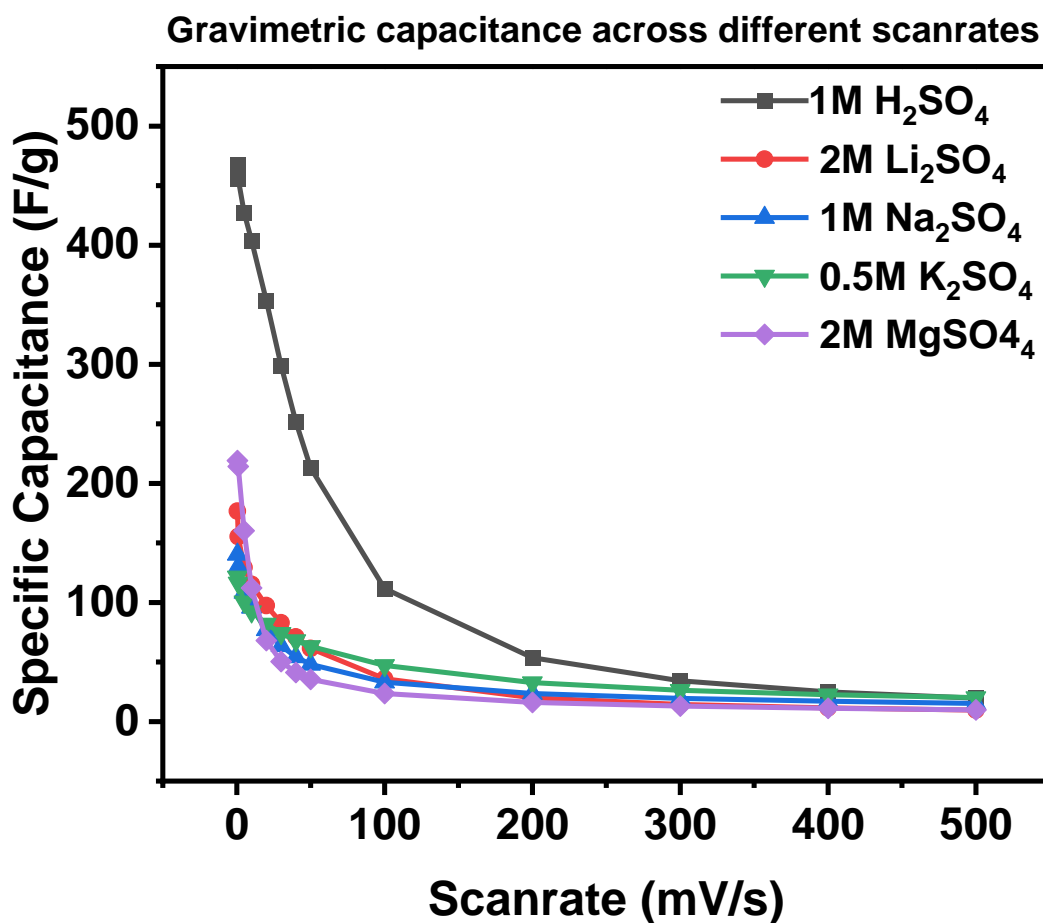
Figure 16: Capacitance vs Potential scan-rate for sulphate based electrolytes

An interesting observation is made from *Figures 12, 14 and 16*; the capacitance values of V_2C in magnesium and aluminium based electrolytes at low scan-rates of $0.5\ mV/s$ and $1\ mV/s$ are best or second to best in their groups. At such low scan-rates, the bulky ions are allowed enough time to overcome their slow kinetics and possibly intercalate at the V_2C interface. In the CVs plotted in *Figure 17*, V_2C clearly shows signs of pseudocapacitance in $2\ M\ MgSO_4$ and $3\ M\ MgCl_2$ aqueous electrolytes.

This activity at slow scan-rates decays rapidly as we increase the scan-rate (*Figure 14, 16*), limiting the performance of V_2C MXene by the sluggish kinetics of the bulky magnesium ion in its hydrated state, inhibiting successful intercalation at high scan-rates.

Observing the measured conductivity values of both these electrolytes, we can comment that the resistive CVs of $3\,M\,MgCl_2$ and $2\,M\,MgSO_4$ in *Figure 13 and 15* respectively, arise due to an electrical resistance as an ionic resistance with such high conductivity values is unlikely.
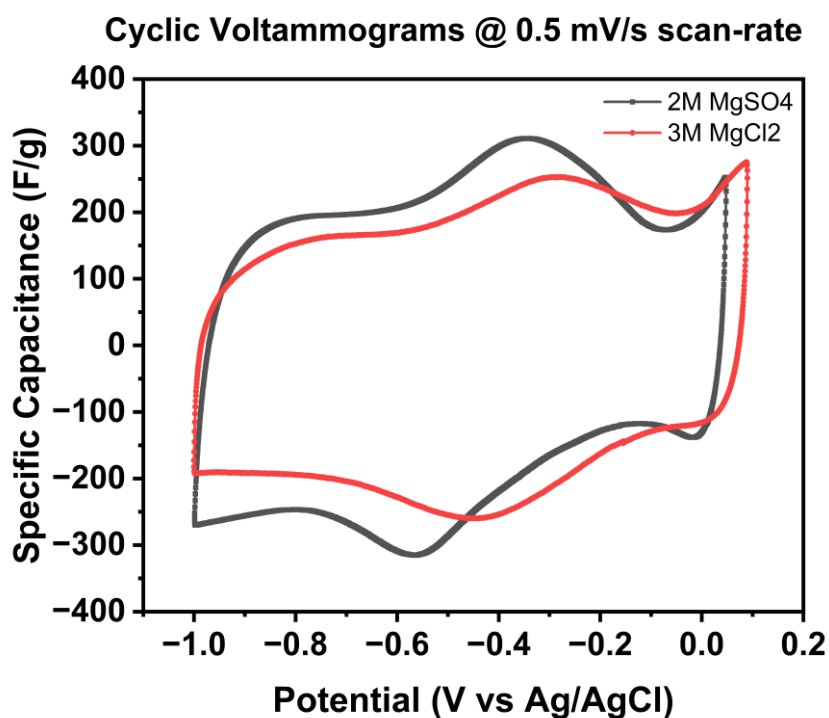
Cyclic Voltammograms @ 0.5 mV/s scan-rate

Figure 17: CVs of V₂C in magnesium ion aqueous electrolytes

In *Figure 15 and 16* we also included the electrolyte $1\,M\,H_2SO_4$ or sulphuric acid in which V_2C has a notably high performance. This result is expected as many other pseudocapacitive materials like Ti_3C_2, RuO_2, etc. are known to perform the best in strong acidic electrolytes. One of the major reasons for this is the small size of the hydronium ion (H_3O^+) which makes it very suitable for fast redox reactions, allowing a faster diffusion and even intercalation in the porous/layered structures of the material. We also measure exceptionally high values of ionic conductivity for concentrated H_2SO_4 solutions allowing for faster kinetics.

This makes sulphuric acid a very suitable electrolyte to study the fundamental redox behavior of a pseudocapacitive material, and thus, we probe deeper into the V_2C MXene electrochemistry.
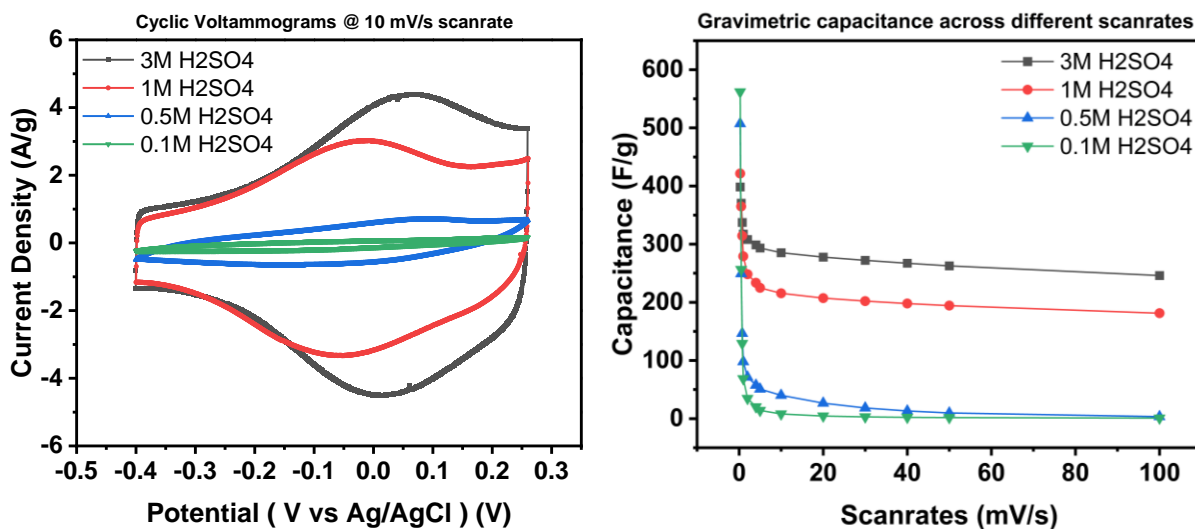
Figure 18: (a)CVs of V₂C in different concentrations of H₂SO₄, (b) Capacitance vs potential scan-rate for in different concentrations of H₂SO₄.

We test V_2C MXene in different concentrations of sulphuric acid and find that $1\,M$ and $3\,M$ concentrations show the best performance at high scanrates (*Figure 18(b)*). The CVs (*Figure 18(a)*) clearly shows deviations from the ideal rectangular shape and these features in the CV are indicative of some pseudocapacitive process taking place in the V_2C MXene. We thus choose sulphuric acid electrolyte to investigate this electrochemistry of V_2C.
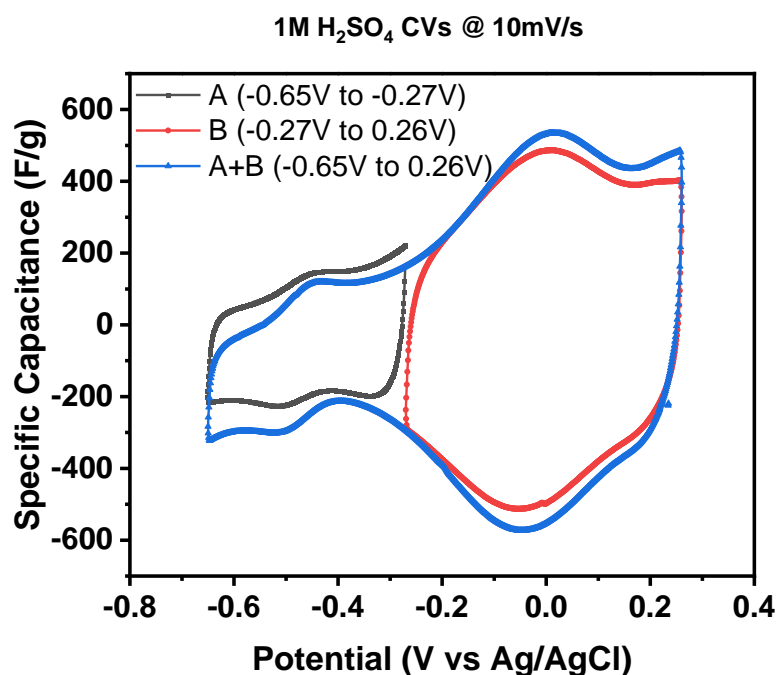
Figure 19: CVs of the different windows A (-0.65V to -0.27V) and B (-0.27V to 0.26V)

Exploring the stable electrochemical window in sulphuric acid shows us a very interesting behavior which is unreported in V_2C literature. Most studies stop at a potential around $-0.4\,V$ vs Ag/AgCl, however, beyond that limit, we observe another pseudocapacitive feature in the CV of V_2C which is only stable and symmetric at scan-rates above $5\,mV/s$. To confirm the existence of the individual pseudocapacitive pairs of peaks, we measure CVs of the individual windows A and B (*Figure 19*), and we find that these two pseudocapacitive faradaic pairs in windows A and B exist independent of each other and have very different stabilities for different concentrations.

Comparison of Cyclic Stability in Window A (-0.65V to -0.27V) & B (-0.27V to 0.26V) @ 10mV/s Scanrate

Figure 20: Comparison of cyclic stability of V_2C in windows A and B of H_2SO_4.

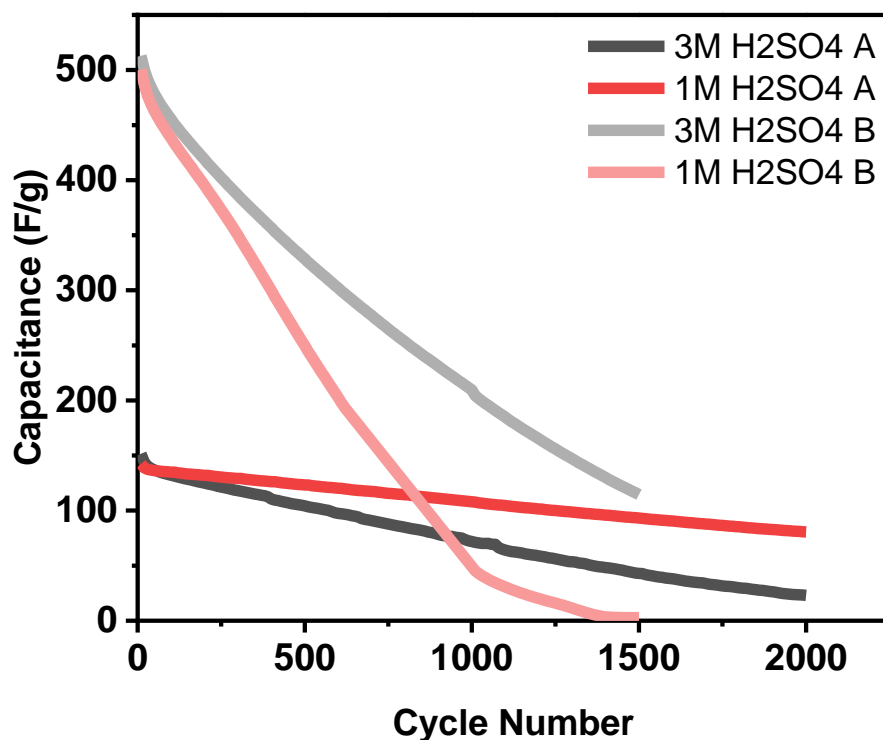*Figure 20* shows the cyclic stability of V_2C in windows A and B of H_2SO_4 for both $1\,M$ and $3\,M$ concentrations. While in window A, V_2C is more stable in $1\,MH_2SO_4$, in window B, in $3\,M\,H_2SO_4$

We suspect the origin of this window dependent electrochemical activity to be from oxidized V_2C, the hypothesis being that in the window A of the highly acidic H_2SO_4, we see the activity of the oxide with lower capacitance and higher stability, whereas, in window B, the activity is shown solely by the V_2C MXene with exceptionally high capacitance but low cyclic stability.

To conclusively prove this hypothesis, we conducted in-situ X-ray Absorption Spectroscopy experiment at a high energy synchrotron X-Ray source, using a specially designed cell with a Kapton window. Results of this experiment are still pending.

The capacitance in window B exceeds all other reports of V_2C and at a scan-rate of $10\,mV/s$, V_2C checks both high capacitance and fast energy storage conditions of the

supercapacitors. However, V_2C MXene has very poor stability in acidic electrolytes as seen in *Figure 20*.

Besides sulphuric acid, V_2C shows a decent capacitance and a good storage at high scan-rate in aqueous lithium and potassium ion electrolytes.

4.4.2 Highly concentrated water in salt electrolytes

Taking into consideration, the trends from aqueous electrolytes, we select some lithium and potassium salts with high enough solubility for preparing highly concentrated water in salt electrolytes (WiSE), keeping in mind the cost and toxicity issue discussed in the introduction.
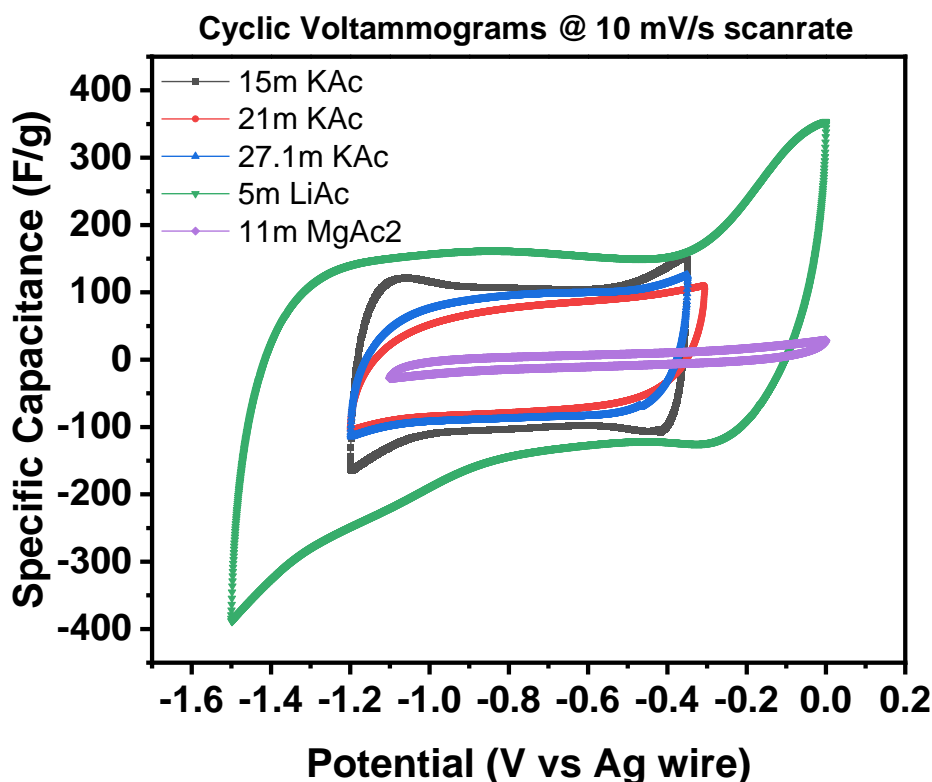

Figure 21: CVs of V₂C in acetate based WiSE.

Among all the acetate based WiSE in *Figure 21*, $5\,m\,LiAc$ and $15\,m\,KAc$ are the electrolytes which the CVs of V_2C match closest to the ideal rectangular shape, with $21\,m\,KAc$ and $27.1\,m\,KAc$ giving nearly ideal V_2C performance and $11\,m\,MgAc_2$ giving

the worst performance of V_2C confirming the initial hypothesis of hinderance in movement of Mg^{2+} ion due to its bulky hydrated state, which is even worse in WiSE because of the increased viscosity from high salt concentrations. *Figure 22* gives further evidence about the relatively higher stability of V_2C at high scan-rates in $5\,m\,LiAc$ and $15\,m\,KAc$ and its poor performance in $11\,m\,MgAc_2$.

The electrochemically stable potential window (ESW) of V_2C in $15\,m\,KAc$ is a mere $0.85\,V$. Among the acetate electrolytes,V_2C has the largest ESW in $5\,m\,LiAc$. Not only a large ESW of $1.5\,V$, $LiAc$ also allows the largest capacitance of V_2C among other acetates.
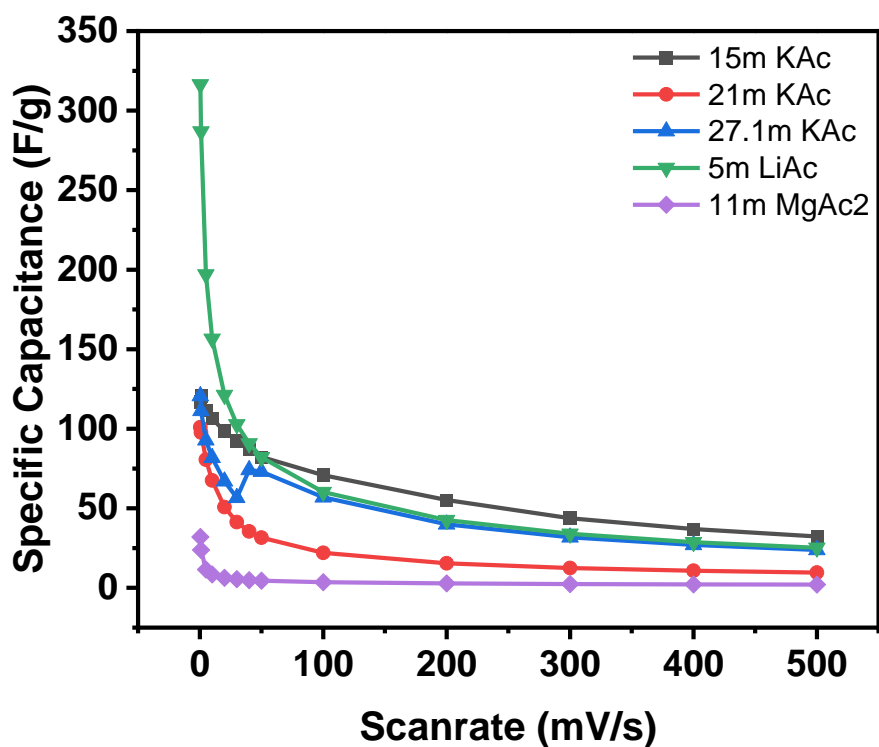
Figure 22:Capacitance vs Potential scan-rate for acetate based WiSE.

Considering the merits of $LiAc$, and Li-ion electrolytes in the general context of this thesis, we try several other Li based WiSE.
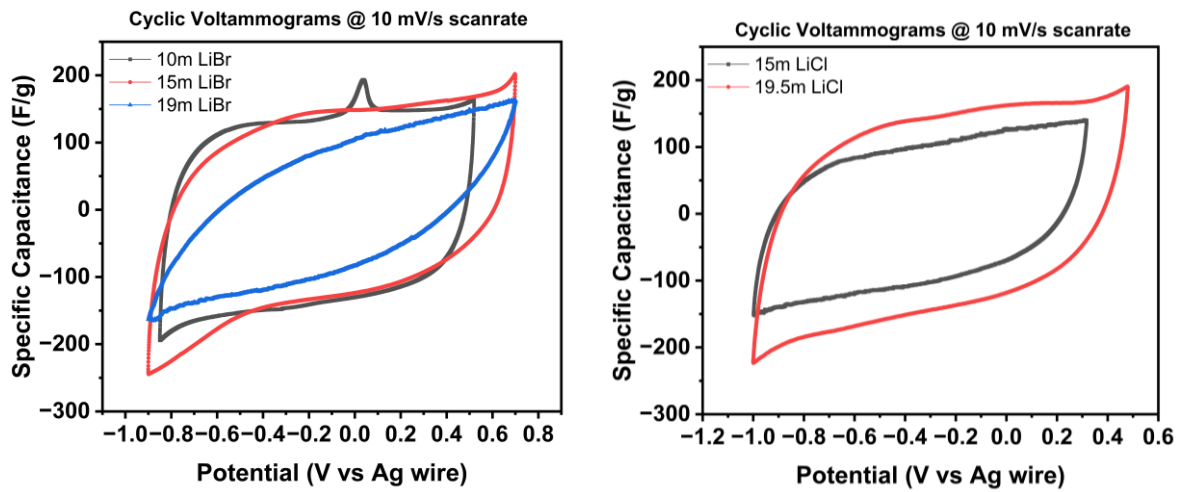
Figure 23: CVs of V2C in LiBr and LiCl solutions of different concentrations.

Figure 23 shows that all of the CVs of V_2C MXene in $LiBr$ and $LiCl$ have an ESW higher than $1.23\,V$. The most resistive CV appears to from $19\,m\,LiBr$, and the largest CV with largest capacitance and ESW was measured in $15\,m\,LiBr$ and $19.5\,m\,LiCl$ among the bromides and chlorides respectively. All other $LiCls$ and $LiBrs$ have considerably large ESWs, decent rate-stability (*Figure 24*), and slightly resistive CVs.
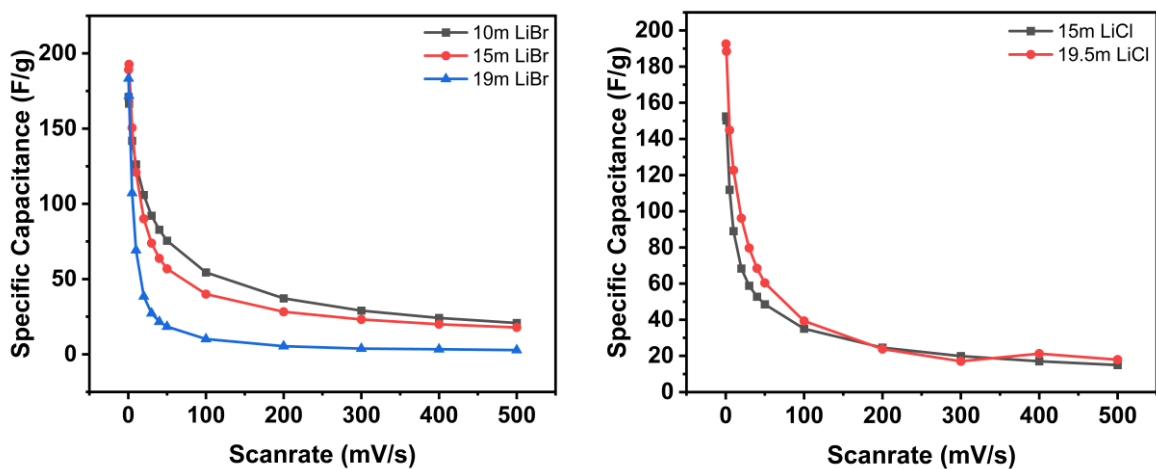
Figure 234: Capacitance vs Scanrate plot for V₂C in lithium ion WiSE.

The huge ESW and capacitance values lead to a very high energy density value for the half cells (*Table 2*) and thus using these lithium ion WiSE we are able to enhance the energy density of V_2C MXene.

Table 2: Energy density of V$_2$C MXene in different WiSE

Electrolyte	Molality (m)	ESW (V)	Capacitance (F/g) @10mV/s	Energy Density (J/g)
KAc	15	0.85	106.38	38.42
$LiAc$	5	1.5	156.6	176.17
$LiCl$	19.5	1.48	122.72	134.4
$LiBr$	15	1.6	120.97	154.84

Selecting $15\,m\,KAc$, $5\,m\,LiAc$, $19.5\,m\,LiCl$ and $15\,m\,LiBr$ as the best concentrations of WiSE in their respective electrolyte groups, we test the cyclic stability of V_2C half-cell at a scan-rate of $10\,mV/s$ in a three-electrode setup.
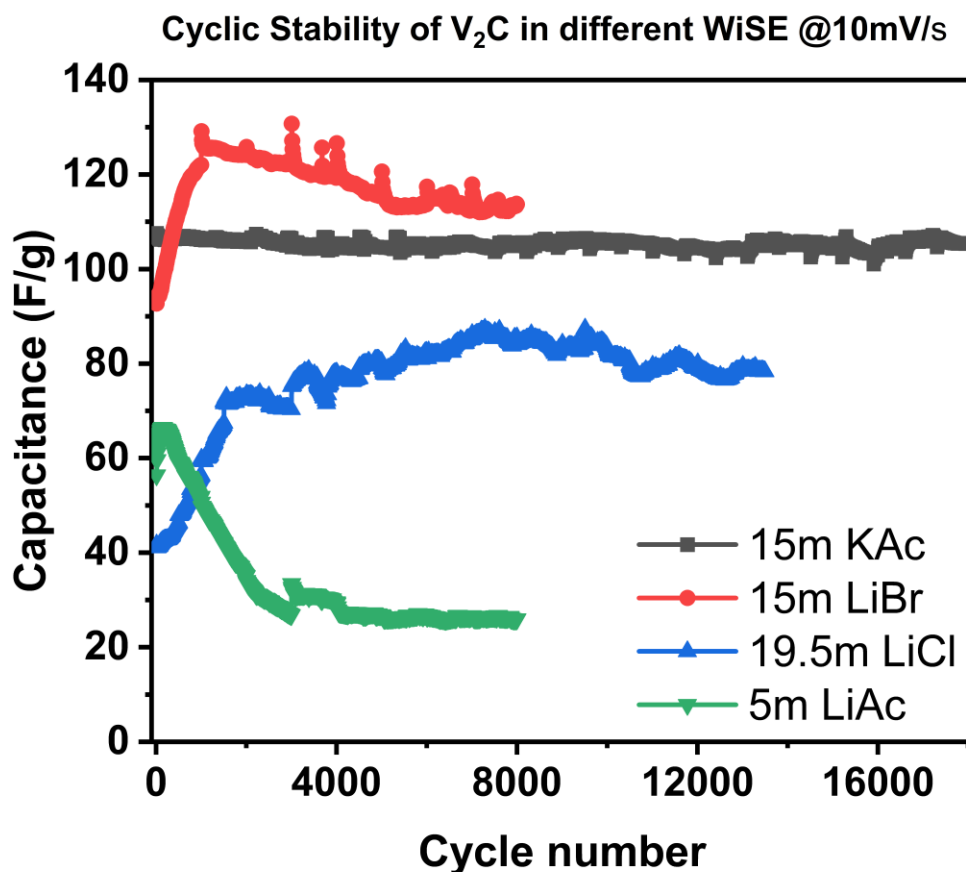
Figure 245: Cyclic stability of V₂C in different WiSE @10mV/s.

We observe in *Figure 25* a remarkable stability of $18,000$ cycles in $15\,m\,KAc$ at a moderately high scanrate of $10\,mV/s$ with less than 10% loss in capacity. Thus, V_2C MXene displays more than satisfactory stability as a pseudocapacitive material with 18,000 charge and discharge cycles through CV technique.

From cycling the V_2C half-cell in lithium ion electrolytes, we observe an electrochemical activation of the material initially from the increasing capacitance values over a few hundred cycles. After the activation cycles in $15m\,LiBr$ and $19.5m\,LiCl$, the value of capacitance doesn't decrease much even after $8,000$ and $14,000$ cycles, but in $5\,m\,LiAc$, we see a huge drop in capacitance right after the activation stage.

5. Conclusions

In this chapter we summarize all the findings about the potential of V_2C MXene as a pseudocapacitive material in different electrolytes, and discuss the suitable conditions for both, the MXene electrode and the electrolytes, based on the experiments conducted in this thesis.

In both $3M$ and $1M$ H_2SO_4, we see an excellent gravimetric capacitance value of over $500\,F/g$ at a scan-rate of $10\,mV/s$, which is higher than any other reported value at this scan-rate. Moreover, we discovered two pairs of pseudocapacitive faradaic peaks in CVs of V_2C, whose independent stabilities and rate performance was studied in separate electrochemical windows, assessed in both $3M$ and $1M$ H_2SO_4.

In addition to exploring the pseudocapacitive behaviour of V_2C MXene in sulphuric acid electrolyte, we also test the activity of V_2C in dilute aqueous electrolytes with a milder pH, and highly concentrated water-in-salt electrolytes.

Some general trends observed in these nitrate, chloride, bromide sulphate and acetate based electrolytes were,

- The corresponding lithium and potassium salts in all of these electrolytes consistently yielded the best capacitive performance from V_2C, among all other electrolytes in their group, with relatively more stability against increasing potential scan-rate.
- Only second to these two ions was sodium, whose electrolytes gave nearly ideal CVs (very slightly resistive), and an intermediate scan-rate performance with V_2C MXene.
- A direct correlation between the electrolyte properties and the rate-stability is difficult to establish as the charge storage kinetics of V_2C in different electrolytes greatly affect the performance at different scan-rates. However, the observed values of capacitance at high and low scan-rates in different electrolytes of the same group (*Table 1*) make perfect sense with the conductivity values measured as explained in *section 4.4*.
- V_2C displayed remarkable cyclic stability with the lithium and potassium based WiSE. Furthermore, all of the lithium ion based WiSE had an ESW

greater than $1.23\ V$, which is a proof of suppressed HER and OER of V_2C in these highly concentrated electrolytes, resulting in expanded windows and huge energy density.

- Lastly, we observe consistently bad performance of V_2C MXene in magnesium salt electrolytes, both aqueous and WiSE, at medium to high scan-rates. This is hypothesized to occur because of the hindered diffusion of bulky solvated divalent Mg^{2+} ion making its kinetics slow. Interestingly, in these same magnesium based electrolytes, V_2C performs well at low scan-rates of $0.5\ mV/s$ and $1\ mV/s$. In all dilute aqueous cases, its capacitance values even surpass the corresponding lithium potassium and sodium salts of its group because of some pseudocapacitive storage at low scan-rates. Thus, even though these electrolytes are less encouraging for rapid storage applications like supercapacitors, they still have huge potential to be used as electrolytes for battery applications.

A thorough study on pseudocapacitive behavior of V_2C MXene was conducted in different electrolytes. Finally, we were able to get half cells with high rate capabilities and huge ESWs using cheap, non-toxic WiSE, thus successfully exploiting the pseudocapacitance of MXene and the expanded ESWs of WiSE to get high energy density electrode systems.

6. Future outlook

Despite the huge capacitance in acidic electrolytes, the cyclic stability of V_2C MXene drops rapidly in these electrolytes. Compared to V_2C, we found that V_4C_3 MXene has significantly better stability in $3\,M\,H_2SO_4$ (*Figure 16*), which implies prospects in not just acidic electrolytes, but other aqueous and WiSE as well.
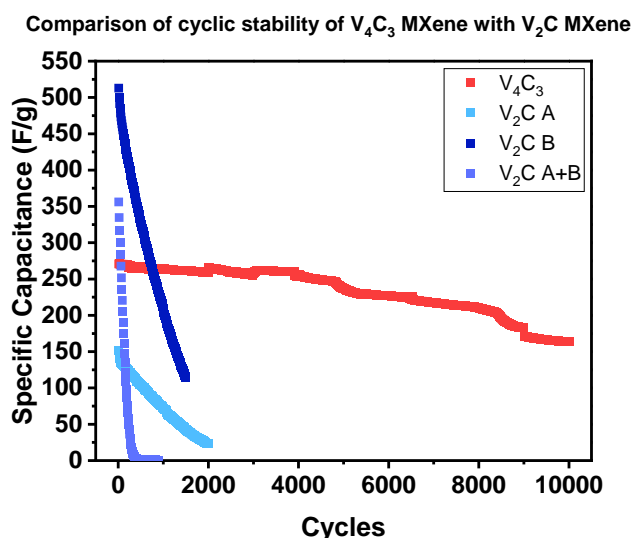

Figure 25: Electrochemical performance of V₄C₃ MXene.

The windows A and B observed in H₂SO₄ and the trends observed with aqueous electrolytes would be understood better if their chemistry is studied using some kind of in-situ characterization technique. This will give us conclusive insights about the nature of V_2C beyond electrochemistry.

The magnesium salt aqueous electrolytes showing exceptional charge storage at low scan rates could have applications in devices with slower kinetics like batteries.

More trends could be found, and performance could be better optimized in WiSE if a bigger range of concentrations of specific WiSE is used for studies.

The expanded ESWs from WiSE can be further exploited by choosing a suitable positive electrode against V_2C MXene to fabricate a high voltage asymmetric full cell.

7. References

(1) Fact.MR 2022, *Increasing Focus on Renewable Energy to Drive Demand for Energy Storage Systems: Fact.MR Study*, GlobeNewswire, accessed 1 October 2022, https://www.globenewswire.com/en/news-release/2022/05/12/2442007/0/en/Increasing-Focus-on-Renewable-Energy-to-Drive-Demand-for-Energy-Storage-Systems-Fact-MR-Study.html

(2) Tan, Y. B.; Lee, J.-M., Graphene for supercapacitor applications. *Journal of Materials Chemistry A* **2013,** *1* (47), 14814-14843.

(3) Simon, P.; Gogotsi, Y., Capacitive Energy Storage in Nanostructured Carbon–Electrolyte Systems. *Accounts of Chemical Research* **2013,** *46* (5), 1094-1103.

(4) Conway, B. E., Transition from "Supercapacitor" to "Battery" Behavior in Electrochemical Energy Storage. *Journal of The Electrochemical Society* **1991,** *138* (6), 1539-1548.

(5) Simon, P.; Gogotsi, Y.; Dunn, B., Where Do Batteries End and Supercapacitors Begin? *Science* **2014,** *343* (6176), 1210-1211.

(6) Lindström, H.; Södergren, S.; Solbrand, A.; Rensmo, H.; Hjelm, J.; Hagfeldt, A.; Lindquist, S.-E., Li+ Ion Insertion in TiO2 (Anatase). 2. Voltammetry on Nanoporous Films. *The Journal of Physical Chemistry B* **1997,** *101* (39), 7717-7722.

(7) Wang, J.; Polleux, J.; Lim, J.; Dunn, B., Pseudocapacitive Contributions to Electrochemical Energy Storage in TiO2 (Anatase) Nanoparticles. *The Journal of Physical Chemistry C* **2007,** *111* (40), 14925-14931.

(8) Chang, L.; Hang Hu, Y., 2.21 Supercapacitors. In *Comprehensive Energy Systems*, Dincer, I., Ed. Elsevier: Oxford, 2018; pp 663-695.

(9) Liu, T.; Li, Y., Addressing the Achilles' heel of pseudocapacitive materials: Long-term stability. *InfoMat* **2020,** *2* (5), 807-842.

(10) Kim, H.; Hong, J.; Park, K.-Y.; Kim, H.; Kim, S.-W.; Kang, K., Aqueous Rechargeable Li and Na Ion Batteries. *Chemical Reviews* **2014,** *114* (23), 11788-11827.

(11) Lukatskaya, M. R.; Feldblyum, J. I.; Mackanic, D. G.; Lissel, F.; Michels, D. L.; Cui, Y.; Bao, Z., Concentrated mixed cation acetate "water-in-salt" solutions as green and low-cost high voltage electrolytes for aqueous batteries. *Energy & Environmental Science* **2018,** *11* (10), 2876-2883.

(12) Naguib, M.; Mochalin, V. N.; Barsoum, M. W.; Gogotsi, Y., 25th Anniversary Article: MXenes: A New Family of Two-Dimensional Materials. *Advanced Materials* **2014,** *26* (7), 992-1005.

(13) Jiang, Q.; Lei, Y.; Liang, H.; Xi, K.; Xia, C.; Alshareef, H. N., Review of MXene electrochemical microsupercapacitors. *Energy Storage Materials* **2020,** *27*, 78-95.

(14) Wang, X.; Mathis, T. S.; Sun, Y.; Tsai, W.-Y.; Shpigel, N.; Shao, H.; Zhang, D.; Hantanasirisakul, K.; Malchik, F.; Balke, N.; Jiang, D.-e.; Simon, P.; Gogotsi, Y., Titanium Carbide MXene Shows an Electrochemical Anomaly in Water-in-Salt Electrolytes. *ACS Nano* **2021,** *15* (9), 15274-15284.

(15) Malchik, F.; Shpigel, N.; Levi, M. D.; Mathis, T. S.; Mor, A.; Gogotsi, Y.; Aurbach, D., Superfast high-energy storage hybrid device composed of MXene and Chevrel-phase electrodes operated in saturated LiCl electrolyte solution. *Journal of Materials Chemistry A* **2019,** *7* (34), 19761-19773.

(16) Anasori, B.; Lukatskaya, M. R.; Gogotsi, Y., 2D metal carbides and nitrides (MXenes) for energy storage. *Nature Reviews Materials* **2017,** *2* (2), 16098.

(17) Lukatskaya, M. R.; Kota, S.; Lin, Z.; Zhao, M.-Q.; Shpigel, N.; Levi, M. D.; Halim, J.; Taberna, P.-L.; Barsoum, M. W.; Simon, P.; Gogotsi, Y., Ultra-high-rate pseudocapacitive energy storage in two-dimensional transition metal carbides. *Nature Energy* **2017,** *2* (8), 17105.

(18) Eames, C.; Islam, M. S., Ion Intercalation into Two-Dimensional Transition-Metal Carbides: Global Screening for New High-Capacity Battery Materials. *Journal of the American Chemical Society* **2014,** *136* (46), 16270-16276.

(19) Wang, J.; Bai, L.; Zhao, X.; Gao, H.; Niu, L., A DFT prediction of two-dimensional MB3 (M = V, Nb, and Ta) monolayers as excellent anode materials for lithium-ion batteries. *RSC Advances* **2022,** *12* (44), 28525-28532.

(20) Shan, Q.; Mu, X.; Alhabeb, M.; Shuck, C. E.; Pang, D.; Zhao, X.; Chu, X.-F.; Wei, Y.; Du, F.; Chen, G.; Gogotsi, Y.; Gao, Y.; Dall'Agnese, Y., Two-dimensional vanadium carbide (V2C) MXene as electrode for supercapacitors with aqueous electrolytes. *Electrochemistry Communications* **2018,** *96*, 103-107.

(21) He, H.; Xia, Q.; Wang, B.; Wang, L.; Hu, Q.; Zhou, A., Two-dimensional vanadium carbide (V2CTx) MXene as supercapacitor electrode in seawater electrolyte. *Chinese Chemical Letters* **2020,** *31* (4), 984-987.

(22) Zahra, S. A.; Anasori, B.; Iqbal, M. Z.; Ravaux, F.; Al Tarawneh, M.; Rizwan, S., Enhanced electrochemical performance of vanadium carbide MXene composites for supercapacitors. *APL Materials* **2022,** *10* (6), 060901.

(23) Song, Y.; Hu, L.; Xin, Y., Nanosized V_2CT_x with Boosting Super Capacitance via Engineering Alkalization Assisted K^+ Interlayer Coordination. *Journal of The Electrochemical Society* **2022,** *169* (7), 072510.

(24) Chen, W.; Zhang, L.; Ren, H.; Miao, T.; Wang, Z.; Zhan, K.; Yang, J.; Zhao, B., V2CTx MXene as novel anode for aqueous asymmetric supercapacitor with superb durability in ZnSO4 electrolyte. *Journal of Colloid and Interface Science* **2022,** *626*, 59-67.

(25) Suo, L.; Borodin, O.; Gao, T.; Olguin, M.; Ho, J.; Fan, X.; Luo, C.; Wang, C.; Xu, K., "Water-in-salt" electrolyte enables high-voltage aqueous lithium-ion chemistries. *Science* **2015,** *350* (6263), 938-43.

(26) Yang, C.; Chen, J.; Qing, T.; Fan, X.; Sun, W.; von Cresce, A.; Ding, M. S.; Borodin, O.; Vatamanu, J.; Schroeder, M. A.; Eidson, N.; Wang, C.; Xu, K., 4.0 V Aqueous Li-Ion Batteries. *Joule* **2017,** *1* (1), 122-132.

(27) Gambou-Bosca, A.; Bélanger, D., Electrochemical characterization of MnO2-based composite in the presence of salt-in-water and water-in-salt electrolytes as electrode for electrochemical capacitors. *Journal of Power Sources* **2016,** *326*, 595-603.

(28) Tribbia, M.; Pianta, N.; Brugnetti, G.; Lorenzi, R.; Ruffo, R., A new double layer super-capacitor made by free-standing activated carbon membranes and highly concentrated potassium acetate solutions. *Electrochimica Acta* **2020,** *364*, 137323.

(29) Lukatskaya, M. R.; Feldblyum, J. I.; Mackanic, D. G.; Lissel, F.; Michels, D. L.; Cui, Y.; Bao, Z., Concentrated mixed cation acetate "water-in-salt" solutions as green and low-cost high voltage electrolytes for aqueous batteries. *Energy & Environmental Science* **2018,** *11* (10), 2876-2883.

(30) Yang, C.; Chen, J.; Ji, X.; Pollard, T. P.; Lü, X.; Sun, C.-J.; Hou, S.; Liu, Q.; Liu, C.; Qing, T.; Wang, Y.; Borodin, O.; Ren, Y.; Xu, K.; Wang, C., Aqueous Li-ion battery enabled by halogen conversion–intercalation chemistry in graphite. *Nature* **2019,** *569* (7755), 245-250.

(31) Turgeman, M.; Wineman-Fisher, V.; Malchik, F.; Saha, A.; Bergman, G.; Gavriel, B.; Penki, T. R.; Nimkar, A.; Baranauskaite, V.; Aviv, H.; Levi, M. D.;

Noked, M.; Major, D. T.; Shpigel, N.; Aurbach, D., A cost-effective water-in-salt electrolyte enables highly stable operation of a 2.15-V aqueous lithium-ion battery. *Cell Reports Physical Science* **2022,** *3* (1), 100688.

(32) Avireddy, H.; Byles, B. W.; Pinto, D.; Delgado Galindo, J. M.; Biendicho, J. J.; Wang, X.; Flox, C.; Crosnier, O.; Brousse, T.; Pomerantseva, E.; Morante, J. R.; Gogotsi, Y., Stable high-voltage aqueous pseudocapacitive energy storage device with slow self-discharge. *Nano Energy* **2019,** *64*, 103961.

(33) Kim, K.; Ando, Y.; Sugahara, A.; Ko, S.; Yamada, Y.; Otani, M.; Okubo, M.; Yamada, A., Dense Charge Accumulation in MXene with a Hydrate-Melt Electrolyte. *Chemistry of Materials* **2019,** *31* (14), 5190-5196.

(34) Kim, K.; Okubo, M.; Yamada, A., Interfacial Dissociation of Contact-Ion-Pair on MXene Electrodes in Concentrated Aqueous Electrolytes. *Journal of The Electrochemical Society* **2019,** *166* (15), A3739-A3744.

(35) Malchik, F.; Shpigel, N.; Levi, M. D.; Mathis, T. S.; Mor, A.; Gogotsi, Y.; Aurbach, D., Superfast high-energy storage hybrid device composed of MXene and Chevrel-phase electrodes operated in saturated LiCl electrolyte solution. *Journal of Materials Chemistry A* **2019,** *7* (34), 19761-19773.

(36) Shpigel, N.; Malchik, F.; Levi, M. D.; Gavriel, B.; Bergman, G.; Tirosh, S.; Leifer, N.; Goobes, G.; Cohen, R.; Weitman, M.; Aviv, H.; Tischler, Y. R.; Aurbach, D.; Gogotsi, Y., New aqueous energy storage devices comprising graphite cathodes, MXene anodes and concentrated sulfuric acid solutions. *Energy Storage Materials* **2020,** *32*, 1-10.

(37) Shpigel, N.; Chakraborty, A.; Malchik, F.; Bergman, G.; Nimkar, A.; Gavriel, B.; Turgeman, M.; Hong, C. N.; Lukatskaya, M. R.; Levi, M. D.; Gogotsi, Y.; Major, D. T.; Aurbach, D., Can Anions Be Inserted into MXene? *Journal of the American Chemical Society* **2021,** *143* (32), 12552-12559.

(38) Wang, X.; Bak, S.-M.; Han, M.; Shuck, C. E.; McHugh, C.; Li, K.; Li, J.; Tang, J.; Gogotsi, Y., Surface Redox Pseudocapacitance of Partially Oxidized Titanium Carbide MXene in Water-in-Salt Electrolyte. *ACS Energy Letters* **2022,** *7* (1), 30-35.

(39) Luo, J.; Ye, S.; Li, T.; Sarnello, E.; Li, H.; Liu, T., Distinctive Trend of Metal Binding Affinity via Hydration Shell Breakage in Nanoconfined Cavity. *The Journal of Physical Chemistry C* **2019,** *123* (23), 14825-14833.

Appendix A

Stable electrochemical window of V_2C MXene is selected in 15m LiBr and 1M (1.02m) LiBr. We observe an expanded window of 1.6 V in WiSE as compared to 1.25 V in dilute aqueous electrolytes.

V_2C ESW selection in LiBr using CVs
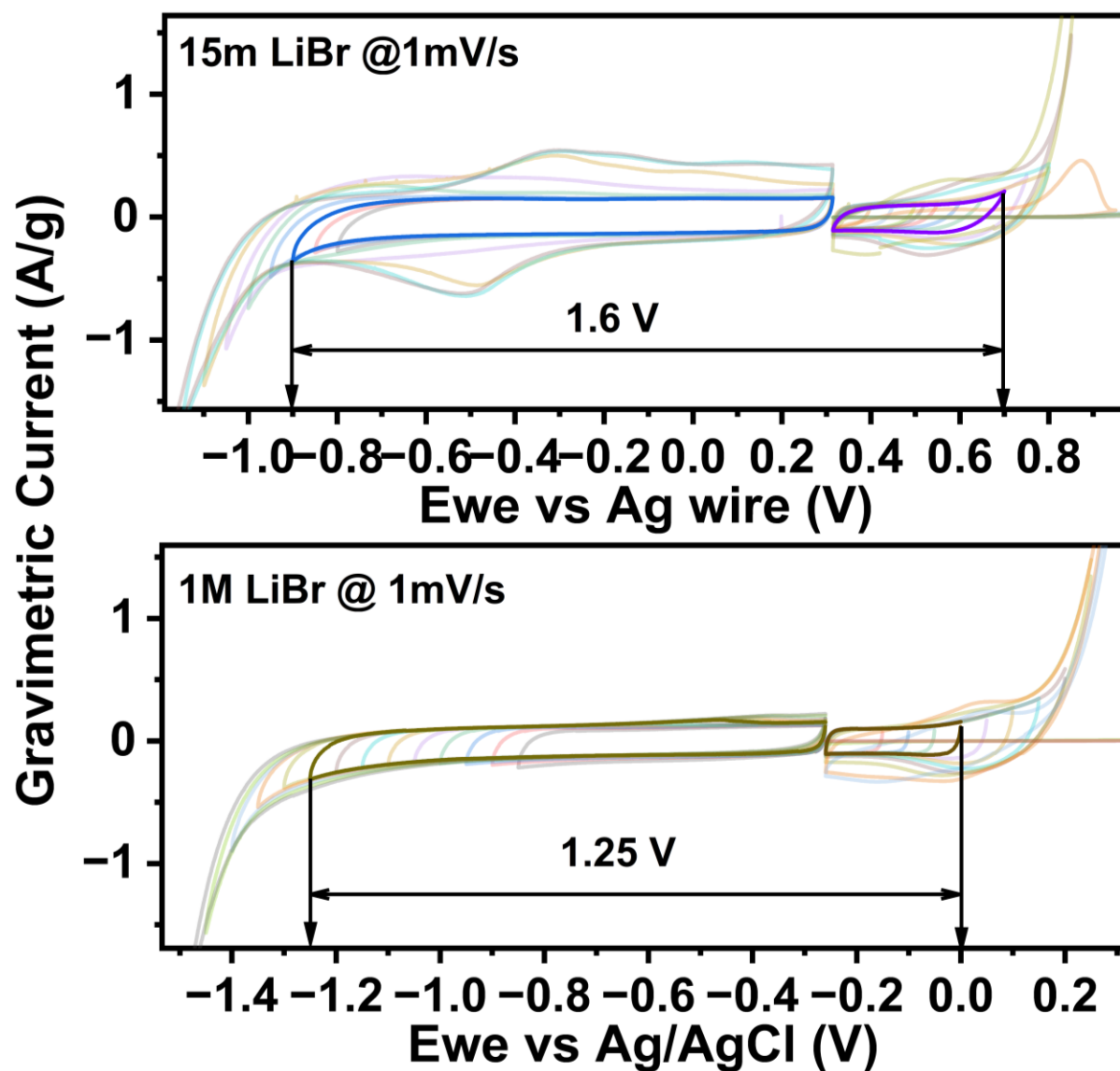
Similarly, we observe an expanded stability window of 1.48 V in 19.5 m LiCl from 1.25V in 5M (5.57 m) LiBr.

The window of 1.25 V in dilute aqueous electrolytes is expected as the water splitting potential is 1.23 V at STP.

V₂C ESW selection in LiCl using CVs